NASA
Technical
Paper
3593

March 1996

A New Correction Technique for Strain-Gage Measurements Acquired in Transient-Temperature Environments

W. Lance Richards

NASA
Technical
Paper
3593

March 1996

A New Correction Technique for Strain-Gage Measurements Acquired in Transient-Temperature Environments

W. Lance Richards

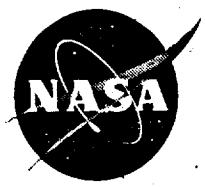

NASA Technical Paper 3593

March 1996

A New Correction Technique for Strain-Gage Measurements Acquired in Transient-Temperature Environments

W. Lance Richards
Dryden Flight Research Center
Edwards, California

National Aeronautics and Space Administration

Office of Management

Scientific and Technical Information Program

CONTENTS

FIGURES

TABLES

ABSTRACT

Significant strain-gage errors may exist in measurements acquired in transient-temperature environments if conventional correction methods are applied. As heating or cooling rates increase, temperature gradients between the strain-gage sensor and substrate surface increase proportionally. These temperature gradients introduce strain-measurement errors that are currently neglected in conventional strain-correction theory and practice. Therefore, the conventional correction theory has been modified to account for these errors. A new experimental method has been developed to correct strain-gage measurements acquired in environments experiencing significant temperature transients. The new correction technique has been demonstrated through a series of tests in which strain measurements were acquired for temperature-rise rates ranging from 1 to greater than 100 °F/sec. Strain-gage data from these tests have been corrected with both the new and conventional methods and then compared with an analysis. Results show that for temperature-rise rates greater than 10 °F/sec the strain measurements corrected with the conventional technique produced strain errors that deviated from analysis by as much as 45 percent, whereas results corrected with the new technique were in good agreement with analytical results.

NOMENCLATURE

a_0, a_1, a_2, a_3	polynomial coefficients
Al	aluminum
CTE	coefficient of thermal expansion, 1×10^{-6}/°F
DACS	data acquisition and control system
E	modulus of elasticity, lb/in^2
GF	gage factor, dimensionless
N_T	thermal force (per unit length), lb/in
M_T	thermal moment (per unit length), (in-lb)/in
Sn	tin
t	thickness, in.
T	temperature, °F
Ti	titanium
x,y	Cartesian coordinates in the plane of the coupon
z	Cartesian coordinate through the thickness of the coupon
α_g	coefficient of thermal expansion of the strain-gage element, 1×10^{-6}/°F
$\alpha_g{}'$	$\alpha_g{}' = \left(\frac{\gamma}{GF} - \alpha_g\right)$, 1×10^{-6}/°F
α_s	coefficient of thermal expansion of substrate material, 1×10^{-6}/°F
γ	temperature coefficient of resistivity, 1×10^{-6}/°F
ΔT_g	temperature change of gage element from initial reference temperature, °F
ΔT_{gs}	temperature difference between gage element and substrate, °F
ΔT_s	temperature change of substrate from initial reference temperature, °F
ε	strain, μstrain
ε_{app}	apparent strain, μstrain
ε_{ind}	indicated strain, μstrain
ε_σ	stress-induced strain, μstrain
$\varepsilon_{T,\dot{T}}$	combined strain error due to temperature, μstrain
$\varepsilon_{\dot{T}}$	transient-temperature strain error, μstrain
ν	Poisson's ratio, dimensionless
σ	stress, lb/in^2

Subscripts

g	gage
gs	difference between gage and substrate
s	substrate
T	temperature
x,y	Cartesian coordinates in the plane of the coupon

Superscript

j	index, 1,2,3, ...

INTRODUCTION

The techniques used to correct strain-gage errors encountered in slowly varying temperature environments are generally well-established and reliable. Highly transient–temperature conditions, however, are required for many current test programs, such as those tests in support of hypersonic or transatmospheric vehicle programs.

Figure 1 shows such a vehicle test component instrumented with a bonded electrical-resistance strain gage. As heating rates applied to a strain-gage installation increase, temperature differences between the strain gage and the substrate will increase according to Fourier's law. These differences (fig. 1) become increasingly significant because the materials used to insulate gages electrically from the substrate are usually good thermal insulators as well. The lower the thermal conductivity of the strain-gage insulating material, the greater the temperature difference through the strain-gage installation (for the same heat flux imposed).

Conventional strain-correction procedures currently neglect temperature gradients by assuming that these temperature differences are insignificant and, therefore, do not adversely affect strain-gage measurement accuracy. This assumption may be valid for slowly varying temperature environments, but it is uncertain at what heating or cooling condition this assumption becomes inappropriate.

Blosser et al. calculated the temperature difference between a strain-gage sensor and a test article surface during a thermal-structural test program.[1] From Fourier's law, a temperature difference of approximately 20 °F was predicted between a strain-gage sensing element and the heated surface of an actively cooled hypersonic structural panel exposed to a 12-Btu/ft^2 sec heating rate. Because no procedures were available in the literature to correct measurements for these temperature differences, the strain-gage measurements on the heated surfaces of the test article were not meaningful.

Limited information is available about correcting electrical-resistance strain-gage measurements obtained in transient-temperature environments. Part of a study that Wilson conducted for the X-15 program evaluated weldable strain gage performance to 900 °F with temperature-rise rates of 1.7, 5, and 10 °F/sec.[2] Adams evaluated the weldable–strain gage response in a heating simulation of a molten sodium spill in a reactor pressure vessel.[3] Temperatures greater than 1000 °F and temperature-rise rates of approximately 100 °F/sec were obtained. These studies, however, only addressed weldable strain gage behavior for a specific measurement problem and employed methods not easily adapted to other test programs. No studies were found in the

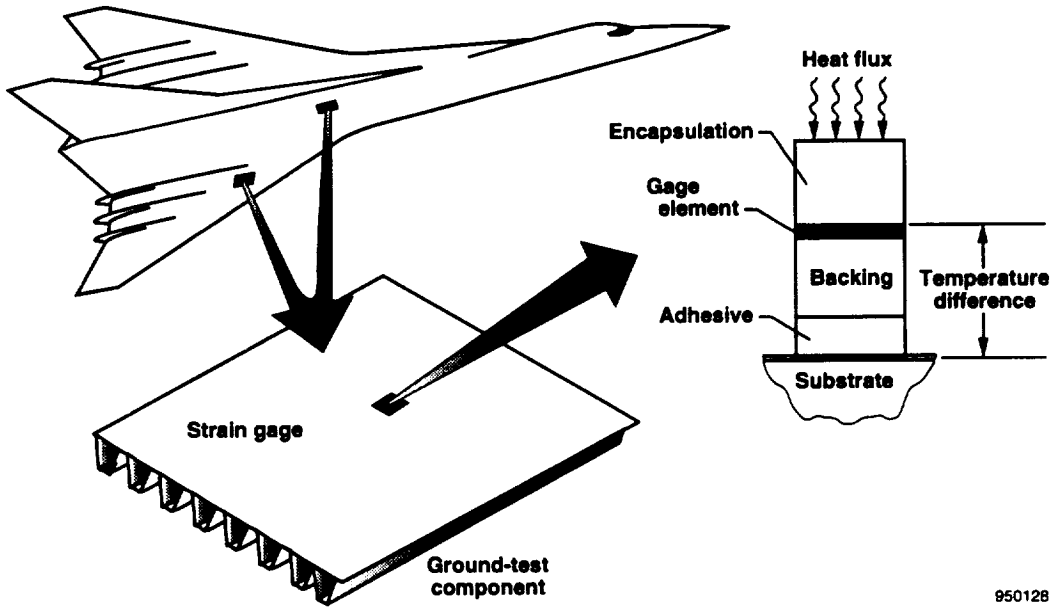

Figure 1. Strain gage installation on a hypersonic vehicle test component.

literature that either define the strain errors produced in transient conditions or provide general techniques to correct errors if they are significant.

In this study, the problem of acquiring strain-gage measurements in transient-temperature environments is readdressed. This paper first reviews the conventional approach to the problem and develops the physical and mathematical foundation for the general heating (or cooling) condition in which the strain-gage sensing element and the substrate temperatures are different. Based on this temperature difference, a new strain-gage measurement error is then mathematically defined. Next, the conventional strain-correction procedure is modified to account for the error. Using a reliable high-temperature foil strain gage, the significance of the error is then experimentally demonstrated for a variety of transient radiant-heating rates. A new correction method, which is developed to be easily applied to other test programs, is provided. Strain results are presented that were obtained with both new and conventional methods. Strain results are also obtained with an analysis that corroborates results obtained with the new method. Use of trade name or names of manufacturers in this report does not constitute an official endorsement of such products or manufacturers, either expressed or implied, by the National Aeronautics and Space Administration.

CONVENTIONAL APPROACH

This section reviews the conventional strain-correction theory by defining the most significant strain errors present in the strain indication acquired in elevated- or cryogenic-temperature environments. The experimental procedures employed to account for these errors are also reviewed.

Strain Correction Theory

The strain-gage indication in extreme temperature environments consists of essentially two components. That is,

$$\varepsilon_{ind}(\Delta T_s^j) = \varepsilon_\sigma(\Delta T_s^j) + \varepsilon_{app}(\Delta T_s^j) \qquad (1)$$

where each term in this equation is expressed as a function of the j^{th} substrate temperature, ΔT_s^j. The first component of the indicated strain, ε_{ind}, is the real, or stress-induced, strain, ε_σ, in the substrate material $\varepsilon_\sigma(\Delta T_s^j)$. The ε_σ term corresponds to the actual stress state of the test article at any given temperature in the substrate-temperature excursion. These strains may result from nonuniform thermal gradients, externally applied mechanical loads, or a combination of both. Ideally, the strain-gage sensor responds only to strains that are stress-induced. In elevated- or cryogenic-temperature environments, however, the gage also responds to apparent strain, $\varepsilon_{app}(\Delta T_s^j)$, the second term in equation (1). This error is defined by the following equation:[4, 5]

$$\varepsilon_{ind}(\Delta T_s^j) = \left[(\alpha_s - \alpha_g) + \frac{\gamma}{GF}\right]\Delta T_s^j \qquad (2)$$

where all terms inside the bracket are also functions of the substrate temperature, ΔT_s^j.*

Figure 2 graphically illustrates the apparent strain error defined in equation (2). The original position of a strain gage and substrate is shown at point A (fig. 2(a)). When an instrumented test article is subjected to a uniform temperature change of the substrate from an initial reference temperature, ΔT_s, the strain gage and the substrate will attempt to expand or contract by an amount corresponding to their coefficients of thermal expansion.

Figure 2(b) shows the resulting thermal expansion of the gage and substrate if both are heated and allowed to expand freely in the positive x direction. In this example, the gage expands to point B (fig. 2(b)), and the substrate expands to point C. Because of its greater stiffness, the substrate will force the gage to conform to its expanded position, as shown at point C (fig. 2(c)). Any local stiffening of the substrate by the gage is neglected. An additional strain of $(\alpha_s - \alpha_g)\Delta T_s$ that is not representative of the stress state in the test article is, therefore, applied to the gage.

---

*Other less significant errors may also exist in the apparent strain, such as gage-factor variation with temperature, Wheatstone-bridge nonlinearity, transverse sensitivity, and lead-wire desensitization. For this investigation, these errors were accounted for using conventional correction methods that are beyond the scope of this study. Further information concerning these errors, or the methods used to correct them, is available in previously published literature.[5–7]

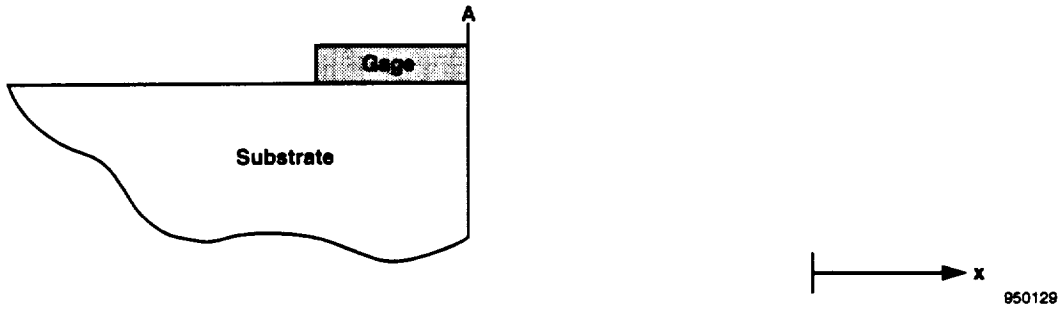

(a) Gage and substrate at ambient condition.

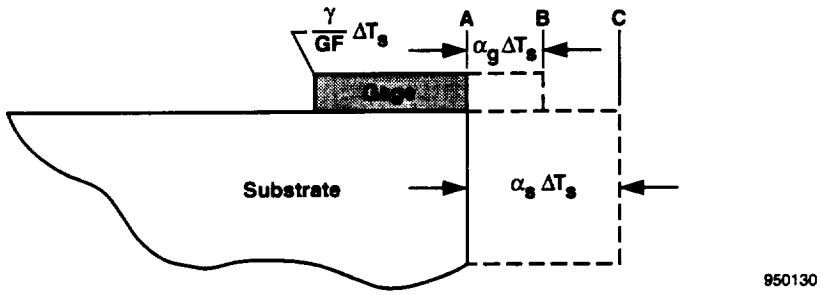

(b) Free thermal expansion of gage and substrate.

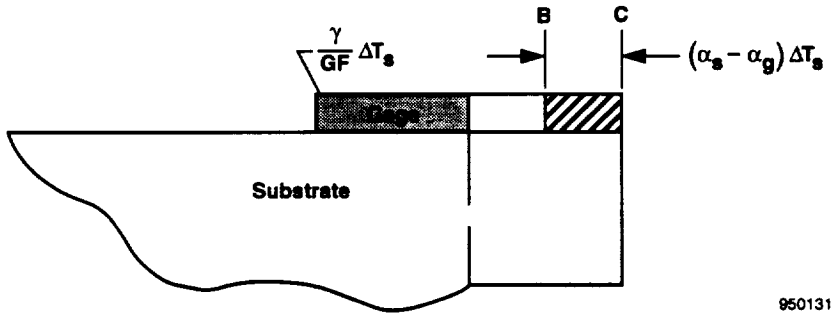

(c) Substrate-induced strain on gage.

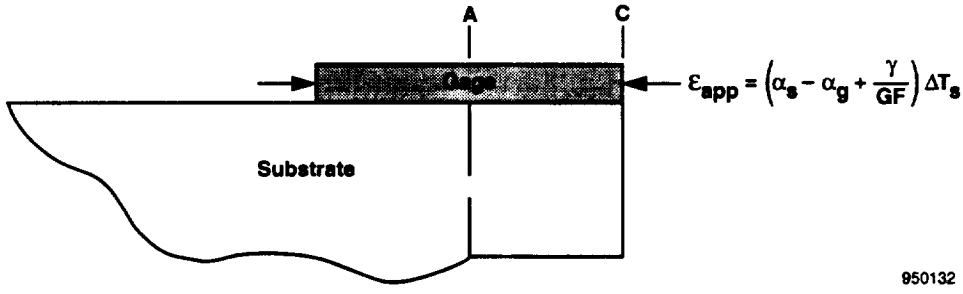

(d) Final state of apparent strain.

Figure 2. Conceptual illustration of apparent strain.

Relative gage-temperature changes also produce changes in the temperature coefficient of resistivity, γ, and the gage factor, GF (figs. 2(b) and 2(c)). Figure 2(d) shows the final stress condition of the gage after responding to free thermal expansion of the substrate. Apparent strain, ε_{app}, as defined in equation (2) and shown graphically in figure 2(d), can not be accurately calculated because considerable variation exists with the temperature dependence of the gage properties from lot to lot. The strain correction procedure described in the following section is relied upon to achieve an accurate correction for the ε_{app} characteristics of the gage.

Strain Correction Procedure

The common technique for characterizing ε_{app} is to first instrument test coupons of the same material as the test article with strain gages of the same lot as those to be used during the tests. Ideally, these coupons have experienced the same manufacturing processes and heat treatments as the test article, so the coupons accurately represent the thermal and physical response characteristics of the test article. The coupon is then placed in an oven and heated slowly to avoid inducing thermal stress in the coupon material. A temperature measurement is required near the strain-gage location to indicate both coupon and gage temperatures.

If the heating rate in the oven is sufficiently slow and the coupon is allowed to freely expand during heating, then the strain-gage output during the temperature profile is ε_{app} as defined in equation (2). The ε_{σ} produced in the test article during an actual test is then determined by subtracting the ε_{app} from the ε_{ind} measurement at the same temperature in the profile, ΔT_s^j. In equation form, this process means simply solving equation (1) for $\varepsilon_{\sigma}(\Delta T_s^j)$:

$$\varepsilon_{\sigma}(\Delta T_s^j) = \varepsilon_{ind}(\Delta T_s^j) - \varepsilon_{app}(\Delta T_s^j) \qquad (3)$$

NEW APPROACH

The conventional approach to correct strain-gage measurements is based on the assumption that the temperature environment varies so slowly that the gage and substrate temperatures remain essentially the same. This section first modifies the conventional correction theory to reflect the more general heating and cooling cases when the gage and the substrate temperatures differ. In addition to the usual strain errors previously discussed, a new error is identified that reflects the strain error produced in transient-temperature environments. After modifying the theory, a new procedure is presented that corrects for the errors obtained in both transient- and isothermal-temperature conditions.

Strain Correction Theory

If heating or cooling rates are severe enough, the strain-gage indication will contain another error resulting from a temperature difference between the substrate and gage materials. The additional error, referred to in this report as the transient-temperature strain error, $\varepsilon_{\dot{T}}$, is added to equation (1).

$$\varepsilon_{ind}(\Delta T_s^j) = \varepsilon_{\sigma}(\Delta T_s^j) + \varepsilon_{app}(\Delta T_s^j) + \varepsilon_{\dot{T}}(\Delta T_s^j) \qquad (4)$$

Because all these terms are functions of the ΔT_s^j, the temperature-dependence expression will not be used in subsequent equations. The last term in equation (4) is determined by first separating the substrate from the gage effects in the ε_{app} expressed in equation (2).

$$\varepsilon_{app} = \underbrace{\alpha_s \Delta T_s}_{\text{substrate}} + \underbrace{\left(\frac{\gamma}{GF} - \alpha_g\right)}_{\text{gage}} \Delta T_s \qquad (5)$$

A temperature difference between the gage element and substrate, ΔT_{gs}, is then added to the gage term of equation (5), and the right-hand side is redefined as the combined strain error due to temperature, $\varepsilon_{T,\dot{T}}$.

$$\varepsilon_{T,\dot{T}} = \underbrace{\alpha_s \Delta T_s}_{\text{substrate}} + \underbrace{\left(\frac{\gamma}{GF} - \alpha_g\right)[\Delta T_s + \Delta T_{gs}]}_{\text{gage}} \qquad (6)$$

After rearranging terms, this equation becomes

$$\varepsilon_{T,\dot{T}} = \left[(\alpha_s - \alpha_g) + \frac{\gamma}{GF}\right]\Delta T_s + \left(\frac{\gamma}{GF} - \alpha_g\right)\Delta T_{gs} \qquad (7)$$

The first half of equation (7) represents the ε_{app} defined in equation (2), and the remaining terms correspond to the $\varepsilon_{\dot{T}}$, or rewritten more simply,

$$\varepsilon_{T,\dot{T}} = \varepsilon_{app} + \varepsilon_{\dot{T}} \tag{8}$$

where

$$\varepsilon_{\dot{T}} = \left(\frac{\gamma}{GF} - \alpha_g\right)\Delta T_{gs} \tag{9}$$

The transient-temperature strain in the above equation can also be illustrated graphically (fig. 3). Figure 3(a) shows the same gage and substrate installation as figure 2(d), with the strain gage subjected to the same ε_{app} error as before. In this example, it is assumed that the installed strain gage is exposed to a highly transient heating profile that produces a positive ΔT_{gs}. In this case, only the gage will respond to the temperature increase by attempting to expand from point C to point D (fig. 3(a)). Because the gage and substrate are bonded together, the substrate will prevent the gage from expanding.

Figure 3(b) shows that, in this example, a compressive strain of $(-\alpha_g)\Delta T_{gs}$ is sensed by the strain gage that is not a result of a ε_σ in the substrate. Gage sensitivity to strain also changes with ΔT_{gs} and further contributes to the $\varepsilon_{\dot{T}}$. Figure 3(c) shows the error and the final equilibrium positions of the gage and substrate.

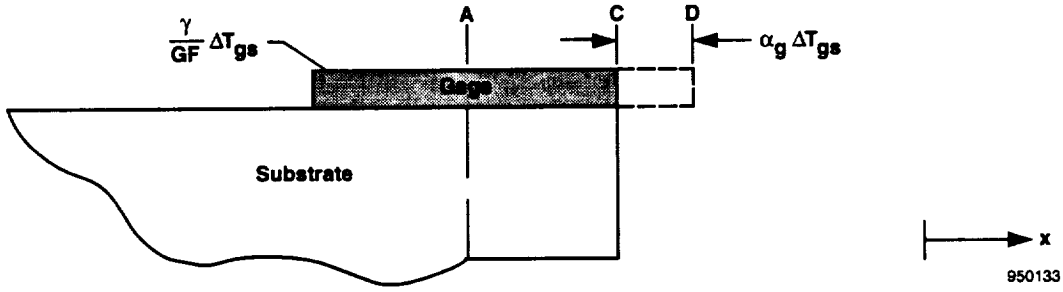

(a) Free thermal expansion of gage due to temperature difference between gage and substrate.

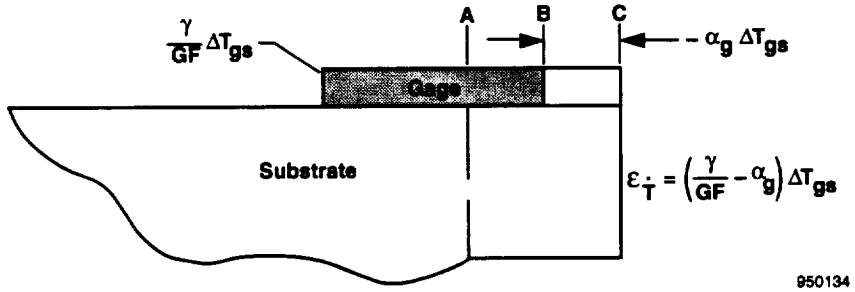

(b) Substrate-induced strain on gage.

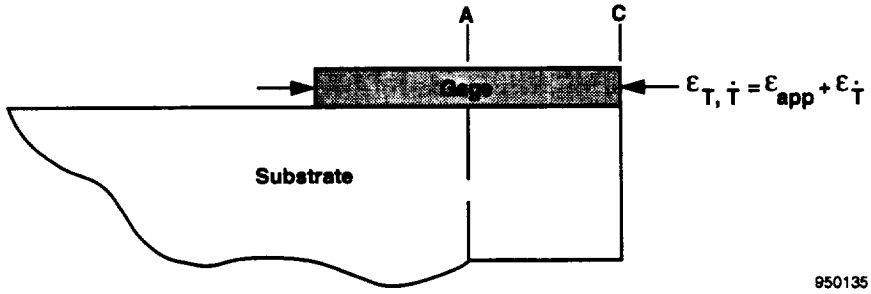

(c) Final stress-state of gage under transient heating conditions.

Figure 3. Conceptual illustration of the transient-temperature strain error.

In the above example, the strain-gage installation was exposed directly to an incident heat flux that produced a positive ΔT_{gs} response through the strain-gage installation. Some transient-temperature conditions, however, involve the transfer of heat in the direction opposite to what was illustrated. Such conditions include the internal heating or the external cooling of the instrumented substrate. These conditions will obviously produce a temperature difference in the opposite sense, and therefore, a negative ΔT_{gs} response. Instead of a positive ΔT_{gs} producing a compressive stress on the gage as before, a negative ΔT_{gs} will now place the strain gage in tension, which also involves a sign change (from negative to positive strain). Therefore, the mathematics accurately represent the physical response of the strain-gage sensor, independent of the direction in which heat is transferred through the installation.

Strain Correction Procedure

In this section, a new procedure is presented with two options to solve for errors developed and described in the previous section. The first option in the new procedure may be used if information concerning the $\varepsilon_{\dot{T}}$ in equation (9) is desired explicitly. However, for computational efficiency, a second option is presented that provides for the straight-forward elimination of both ε_{app} and the $\varepsilon_{\dot{T}}$ simultaneously without having to solve for the $\varepsilon_{\dot{T}}$ first. This option empirically solves for the $\varepsilon_{T,\dot{T}}$ in equation (7). However, both options in the new correction procedure assume that the ε_{app} error in equation (2) has already been determined through the conventional method previously described; that empirical data concerning the substrate coefficient of thermal expansion, α_s, as a function of temperature are available; and that an indication of the strain-gage element temperature is acquired during the course of the actual transient-temperature test.

Transient-Temperature Strain Error Option

In its present form, the $\varepsilon_{\dot{T}}$ in equation (9) can not be solved accurately because the gage properties vary so significantly from one lot of strain gages to another. To accurately solve for the $\varepsilon_{\dot{T}}$, equation (9) must be expressed in a form that lends itself to an empirical solution. This form can be achieved by first grouping the gage coefficients together with the following definition:

$$\alpha_g' = \frac{\gamma}{GF} - \alpha_g \tag{10}$$

Substituting this expression into equations (5) and (9), the ε_{app} becomes

$$\varepsilon_{app} = \underbrace{\alpha_s \Delta T_s}_{\text{substrate}} + \underbrace{\alpha_g' \Delta T_s}_{\text{gage}} \tag{11}$$

and the $\varepsilon_{\dot{T}}$ becomes

$$\varepsilon_{\dot{T}} = \alpha_g' \Delta T_{gs} \tag{12}$$

This equation clearly shows that the $\varepsilon_{\dot{T}}$ is thermal stress–induced and is therefore simply the product of the coefficient of thermal expansion of the strain gage and the temperature difference between the gage and the substrate. To solve directly for the $\varepsilon_{\dot{T}}$ above, the α_g' term is first determined for each substrate temperature from the ε_{app} expressed in equation (11). This term becomes

$$\alpha_g' = \frac{\varepsilon_{app}}{\Delta T_s} - \alpha_s \tag{13}$$

Substituting equation (13) into equation (12), the $\varepsilon_{\dot{T}}$ now becomes

$$\varepsilon_{\dot{T}} = \left(\frac{\varepsilon_{app}}{\Delta T_s} - \alpha_s \right) \Delta T_{gs} \tag{14}$$

Equation (14) allows the $\varepsilon_{\dot{T}}$ to be solved entirely with empirically determined information. The ε_{app} can be accurately determined using conventional methods. The α_s can be obtained from empirically determined handbook data. The ΔT_{gs} term can be determined through measurements of strain-gage and substrate temperatures (ΔT_g and ΔT_s, respectively) during a transient-temperature test.

The ε_σ in equation (4) can now be solved because all the significant errors occurring in highly transient–temperature environments have been determined.

$$\varepsilon_\sigma = \varepsilon_{ind} - \varepsilon_{app} - \varepsilon_{\dot{T}} \tag{15}$$

Combined Strain Error Option

To reduce the number of steps in the computational process, the $\varepsilon_{T,\dot{T}}$ term, which incorporates both slowly varying– and transient-temperature strain errors, can be solved without first having to determine the $\varepsilon_{\dot{T}}$. This procedure is useful if it is desired to automate this process in a data reduction routine. This option is determined by expressing the temperature difference between the gage and substrate as

$$\Delta T_{gs} = \Delta T_g - \Delta T_s \tag{16}$$

Solving for ΔT_s, introducing the result into equation (7), and using the ε_{app} relationship in equation (2), the following equation results:

$$\varepsilon_{T,\dot{T}} = \varepsilon_{app}\left(\frac{\Delta T_g}{\Delta T_s}\right) - \alpha_s \Delta T_{gs} \tag{17}$$

Because this error is a combination of the ε_{app} and the $\varepsilon_{\dot{T}}$ as shown in equation (8), it can be subtracted directly from the ε_{ind} at each substrate temperature in the transient-temperature test to obtain ε_σ:

$$\varepsilon_\sigma = \varepsilon_{ind} - \varepsilon_{T,\dot{T}} \tag{18}$$

Although both correction options were derived to include transient-temperature effects, they are equally appropriate for purely isothermal conditions. Equation (14) shows that as the temperature environment moves from a transient- to isothermal-temperature condition, the ΔT_{gs} term approaches zero, thus causing the $\varepsilon_{\dot{T}}$ to approach zero. For the second procedure, equation (17) shows that as the temperature environment approaches isothermal conditions, the ΔT_{gs} term again approaches zero, and the parenthetic term approaches unity. Therefore, both options in the new procedure approach the conventional procedure as the transient-temperature environment approaches isothermal conditions.

COMPARISON OF THE NEW AND CONVENTIONAL PROCEDURES

Figure 4 shows a flow chart that compares the new and conventional procedures. The conventional correction procedure is shown on the left-hand side of figure 4. The new procedure is shown on the right, and the steps that both procedures have in common are shown in the center.

The first step in both correction procedures is to characterize the ε_{app} using the conventional methods described previously. Once the ε_{app} error is defined, the next step is to instrument the actual test article with strain gages and temperature sensors as required. The new correction method requires some indication of the strain-gage filament temperature, ΔT_g, during the transient-heating tests. The thermal characteristics through the thickness of this temperature sensor should represent the characteristics of the strain-gage sensor.

The next step for both procedures shown in figure 4 is to conduct the transient-heating tests on the test article. Both procedures acquire measurements of ε_{ind} and ΔT_s during the profile; the new method also acquires measurements of ΔT_g. The last step in the conventional procedure is to solve equation (3) by simply subtracting the ε_{app} from the ε_{ind} at every sample of ΔT_s.

The new procedure, however, first determines ΔT_{gs} at each temperature ΔT_s, as shown in equation (16). Then the ΔT_{gs} term, ε_{app}, and α_s are input parameters for both new options, as shown in figure 4.

The first option uses the above input to calculate the $\varepsilon_{\dot{T}}$ in equation (14) and determines the ε_σ from equation (15). The second option in the new procedure uses the same input parameters to directly determine the $\varepsilon_{T,\dot{T}}$ from equation (17). The option obtains the same ε_σ result as the first option but uses equation (18).

TEST DESCRIPTION

A series of tests were conducted to demonstrate the new correction theory and experimental procedures

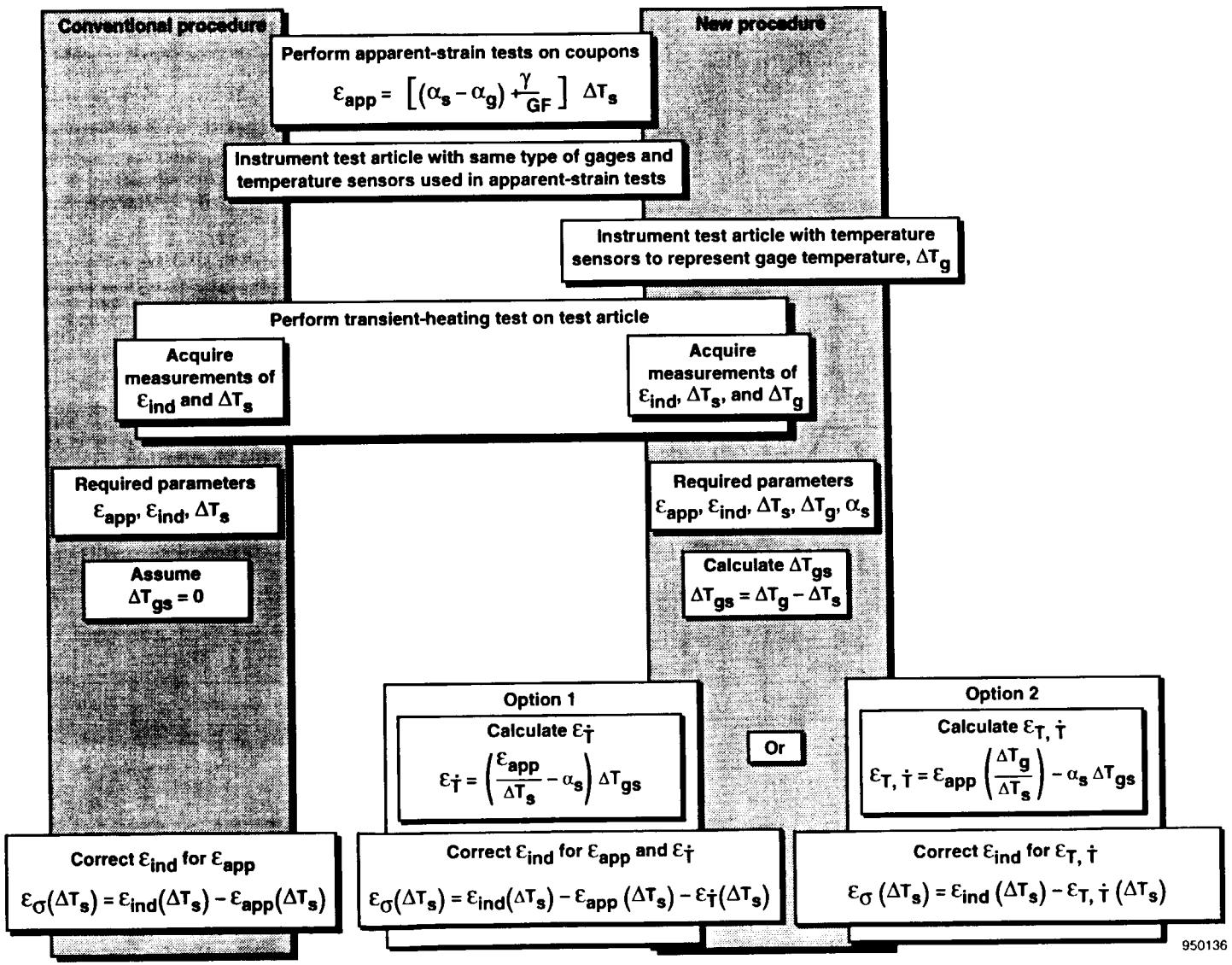

Figure 4. New and conventional correction procedures.

introduced in the previous section. This section describes the test setup, test coupon and instrumentation, data acquisition system, and test matrix used in the experiment.

Test Coupon and Instrumentation

First, a titanium coupon (Ti 5Al-2.5Sn) measuring 3 × 5 × 0.25 in. was used in tests to characterize the ε_{app}. The same coupon also served as the test article in transient-heating tests.

For the ε_{app} tests, the coupon was instrumented with type-K thermocouples and Measurements Group (Raleigh, North Carolina) foil strain gages (WK-05-125BZ-10C) (fig. 5). The rectangular strain-gage rosette shown in the middle of the coupon was installed to provide an adequate statistical representation of the ε_{app} error. The spot-welded thermocouple

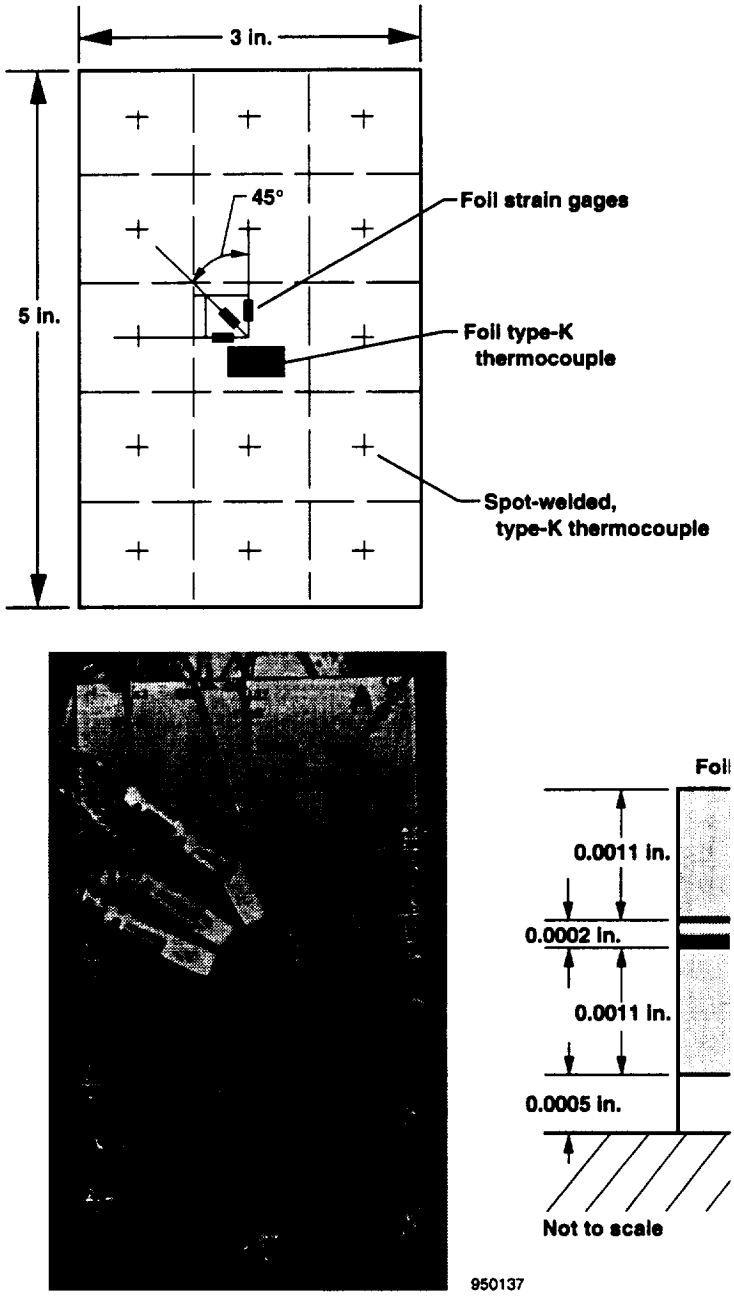

Figure 5. Test coupon and instrumentation.

at the intersection of the three strain axes is normally assumed to measure the strain-gage temperatures for isothermal ε_{app} tests. The gage installation, together with its corresponding thermocouple, is typical of those used in isothermal ε_{app} tests.

In addition to the instrumentation described above, the transient-temperature tests required an indication of the gage temperature during the tests. In this approach, the gage temperature was represented by installing commercially available type-K foil thermocouples (RdF Corporation, Hudson, New Hampshire) (fig. 5) to the substrate using the same attachment materials and techniques as the foil strain gages. The foil thermocouple was assumed to measure the ΔT_g because of its similarity in materials and cross-sectional dimensions to the strain gage (fig. 6).*[8]

Figure 6 shows that the foil strain-gage and foil thermocouple characteristics are nearly identical through their thicknesses. A simple one-dimensional thermal analysis showed that the difference between the strain-gage and foil thermocouple temperatures for a given heat flux was less than 5 percent. The difference between the foil and spot-welded thermocouple measurements was used to define the ΔT_{gs} term in the ε_T (equation (14)).

All sensors on the top surface of the coupon (fig. 5) have corresponding sensors located on the bottom surface. A total of 30 spot-welded thermocouples, 2 foil thermocouples, and 6 foil strain gages were used in the tests. After the sensors were installed, the instrumented coupon (fig. 5) was painted with a high-emittance paint that is not pictured. This paint helped to ensure that a uniform heat flux was applied to the coupon surface and also helped to improve the radiative heating efficiency.

Data Acquisition and Control System

Figure 7 shows a schematic of the data acquisition and control system (DACS)[9] used in the experiments. Signal conditioning, sensor calibration, and thermal control were performed with this system. The DACS controls the coupon surface temperature (closed loop) or the power from the lamps (open loop). In closed-loop mode, a feedback control algorithm adaptively controls the temperature on the coupon. Every 0.25 sec, a thermal control computer compares the temperature of a feedback/control thermocouple on the coupon with a temperature profile prescribed before the test. If the temperature deviates from the programmed temperature profile, a thermal control computer sends the appropriate firing commands to power controllers. The power controllers regulate the firing frequency of radiant quartz lamps until the proper temperature on the coupon is attained.

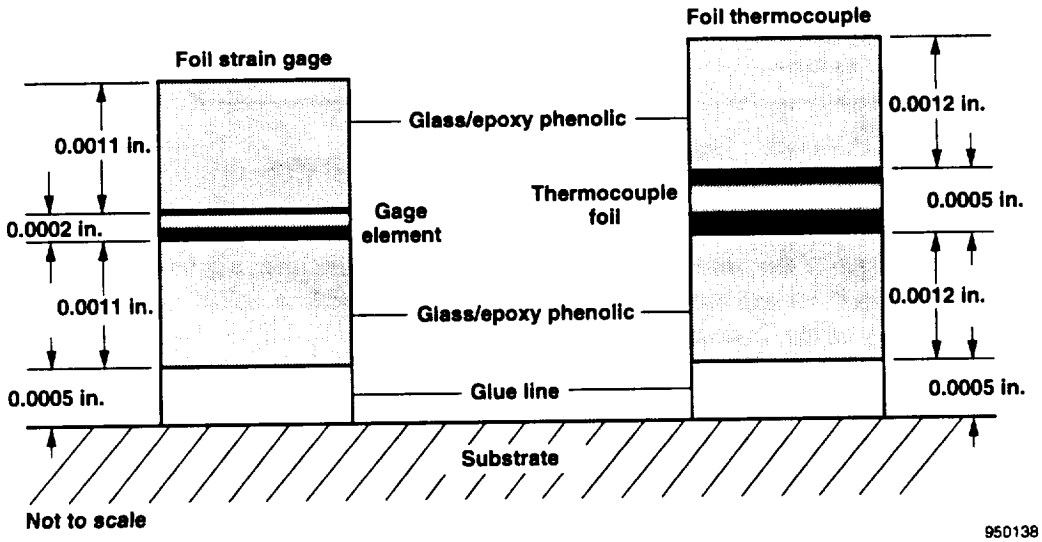

Figure 6. Comparison of foil strain gage and foil thermocouple cross-sections.

*Personal correspondence from Howard J. Howland, Measurements Group, Inc., Raleigh, North Carolina, Aug. 7, 1992.

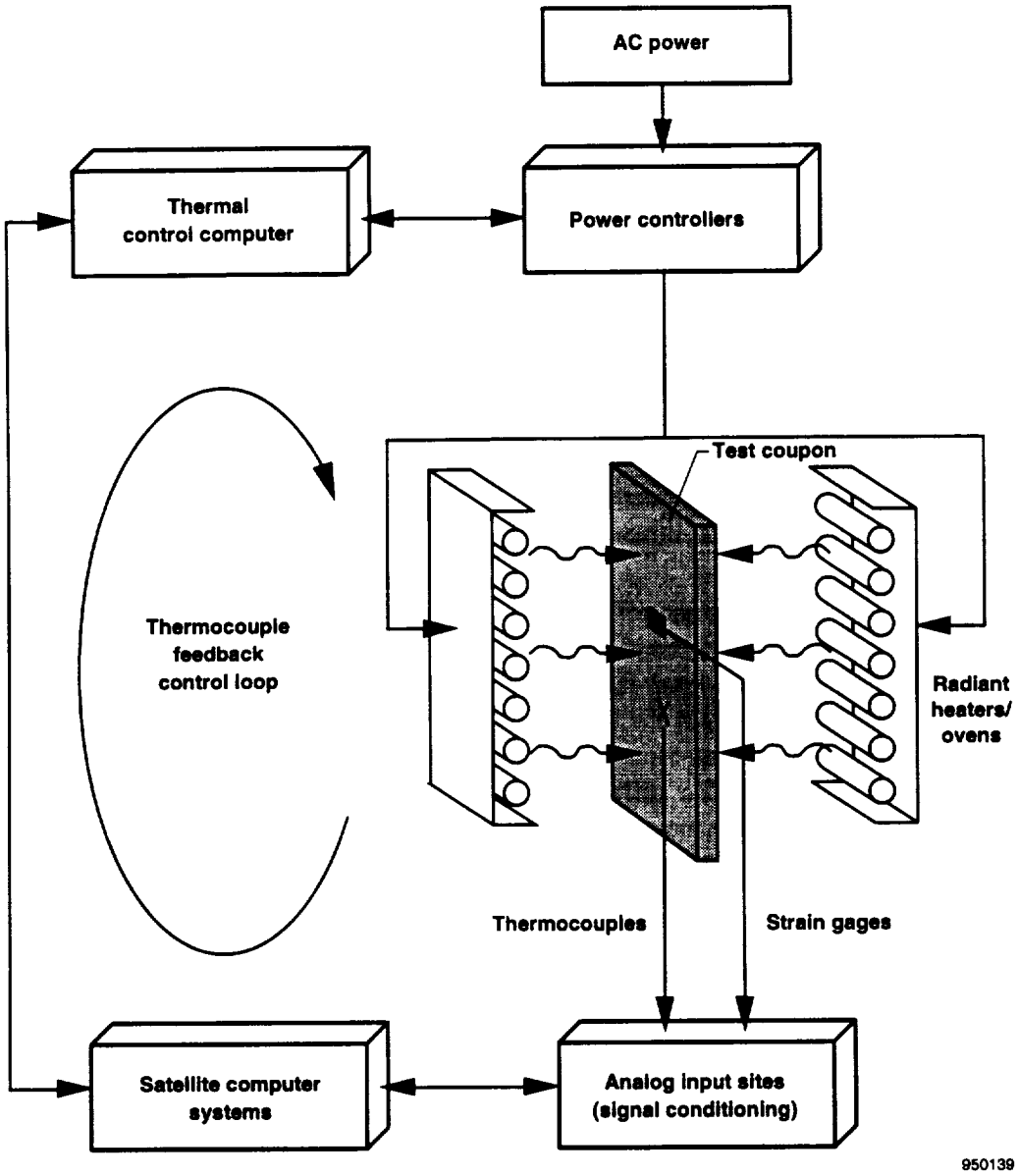

Figure 7. Data acquisition and control system.

A spot-welded thermocouple in the center of the coupon was used in the feedback control loop to control the temperature time-history of the front and back surfaces of the coupon. Both surfaces were programmed to the same temperature time-history, so the coupon would be heated symmetrically about its midplane.

The maximum allowable system measurement error of the DACS is ±0.15 percent of reading or ±0.20 μV, whichever is greater. Therefore, for a ±0.20-μV strain measurement input from a single-active-arm gage with a 4-V direct current excitation voltage, the error is ±8 μstrain. Similarly, a type-K thermocouple measurement error with a ±0.20-μV input is equivalent to ±0.9 °F.[9]

Test Setup

Two ovens were required for heating tests: one for low temperature-rise rates to ensure slow, uniform heating, and a second one capable of achieving temperature-rise rates greater than 100 °F/sec. Figure 8

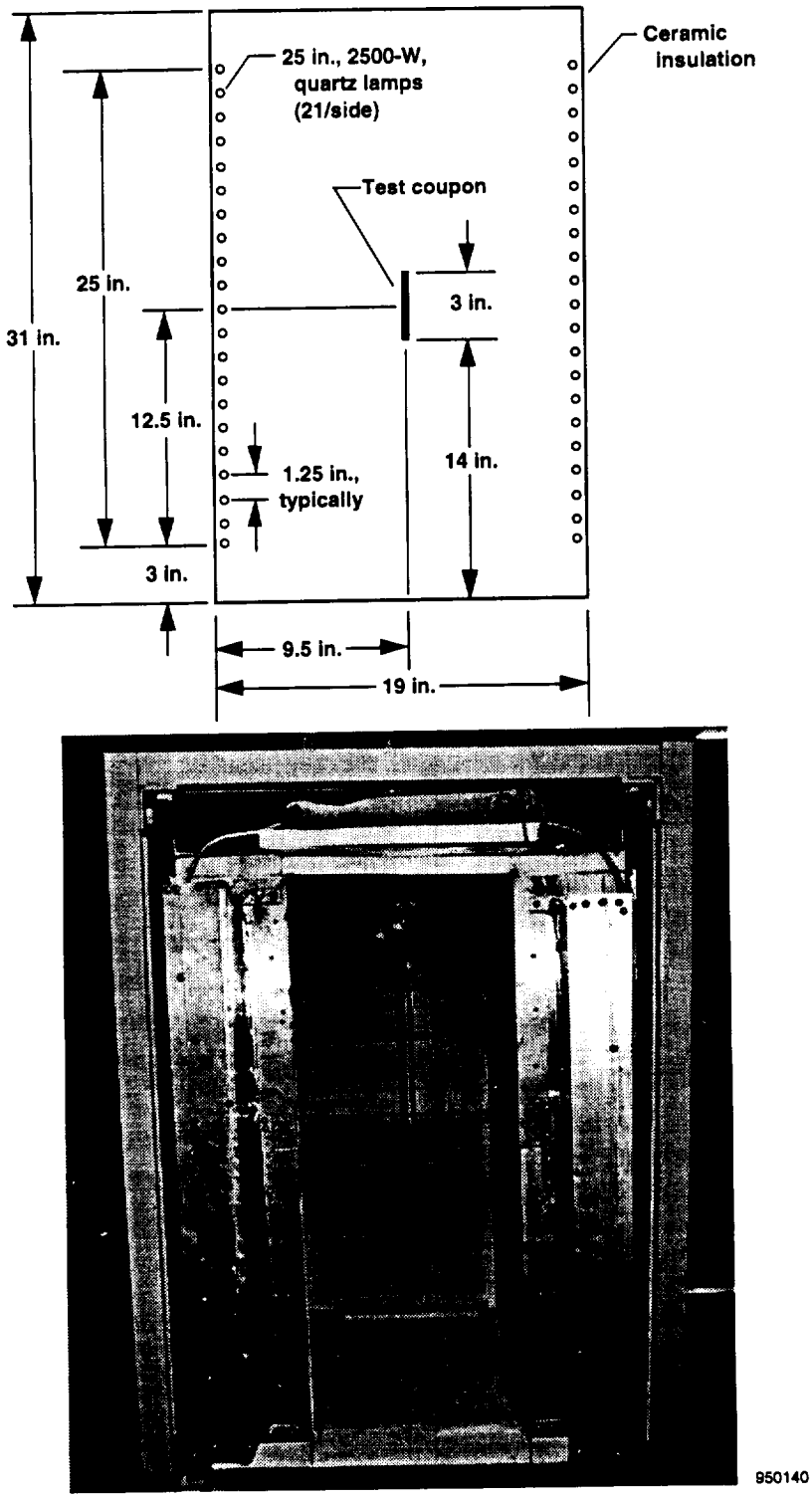

Figure 8. Low heating rate oven.

shows the ceramic oven used for the tests involving temperature-rise rates of less than 20 °F/sec. Heat was applied to both sides of the coupon by 42 quartz infrared lamps (21 per side) spaced 1.25 in. apart. Each lamp provided a maximum of 2500 W at 440 V. All surfaces of the oven were ceramic. Steel baffles were inserted between the coupon and the heating elements for the 0.3 °F/sec test to diffuse heat uniformly to the coupon.

Figure 9 shows the oven used for tests requiring high temperature-rise rates (between 20 and 100 °F/sec). The test coupon was mounted vertically on an insulated stainless steel frame to provide stability and prevent lead wire damage during heating. The maneuverability of the frame within the oven also facilitated accurate coupon orientation between the two banks of parallel lamps. Each side of the coupon was heated by 14 quartz lamps spaced 1 in. apart. Each lamp was capable of producing power greater than 6000 W at 440 V (double the rated voltage). Water/glycol–cooled aluminum reflectors were used to reflect radiant heat to the coupon surfaces. The oven was enclosed with 1.5 in.–thick ceramic blocks, each lined with 0.001 in.–thick nickel foil to improve the oven wall reflectivity.

Test Matrix

Table 1 provides information about the various transient-temperature tests performed. The strain data for the 0.3 °F/sec tests were obtained using conventional correction methods and were used as the baseline ε_{app} correction for subsequent tests. The coupon was heated by convection for the 0.3 °F/sec tests and by radiation for all transient-heating tests. The data sampling rate, initially at 1 sample/sec for the 0.3 °F/sec tests, was increased to 12 samples/sec and eventually to 144 samples/sec to acquire sufficient data samples at the higher transient-temperature conditions.

TEST RESULTS AND DISCUSSION

This section first provides an example of how the new and conventional data correction procedures are used in determining the ε_σ values in a coupon subjected to highly transient–temperature conditions. A heating test with poor thermal control is used to illustrate the data correction procedures for a less than ideal test case. Then, the transient-temperature strain errors from a single, representative test for each of the temperature-rise rates between 10 and 100 °F/sec are presented. Transient-temperature strain errors for tests with heating rates less than or equal to 5 °F/sec were found to be negligible and are, therefore, not presented.

Example of Data Correction Procedures

To help demonstrate the new and conventional procedures, the flow chart presented in figure 4 will be followed by using data obtained from an actual transient-heating test. According to the flow chart, the data correction process begins by first characterizing the ε_{app}. This step was satisfied by placing the instrumented titanium coupon in an oven and heating it several times along a slow, 0.3 °F/sec temperature profile. These tests are part of the test matrix shown in table 1. Three additional 0.3 °F/sec tests were performed on the coupon to adequately represent the ε_{app} response. Figure 10 shows the least-squares curve fit of the ε_{app} and measurement scatter for a single gage for the three 600 °F thermal cycle tests.

In this study, the same instrumented test coupon, described earlier, served as both the ε_{app} coupon and the test article for the transient-heating tests. Therefore, the second step in figure 4 was not necessary.

Table 1. Pertinent test information as a function of nominal temperature-rise rate.

	Nominal temperature-rise rate, °F/sec							
Test information	0.3	1	5	10	20	40	80	100
Number of tests	4	4	5	6	5	5	4	2
Maximum temperature, °F	600	600	600	600	600	500	450	400
Sampling rate/sec	1	12	12	12	12	144	144	144

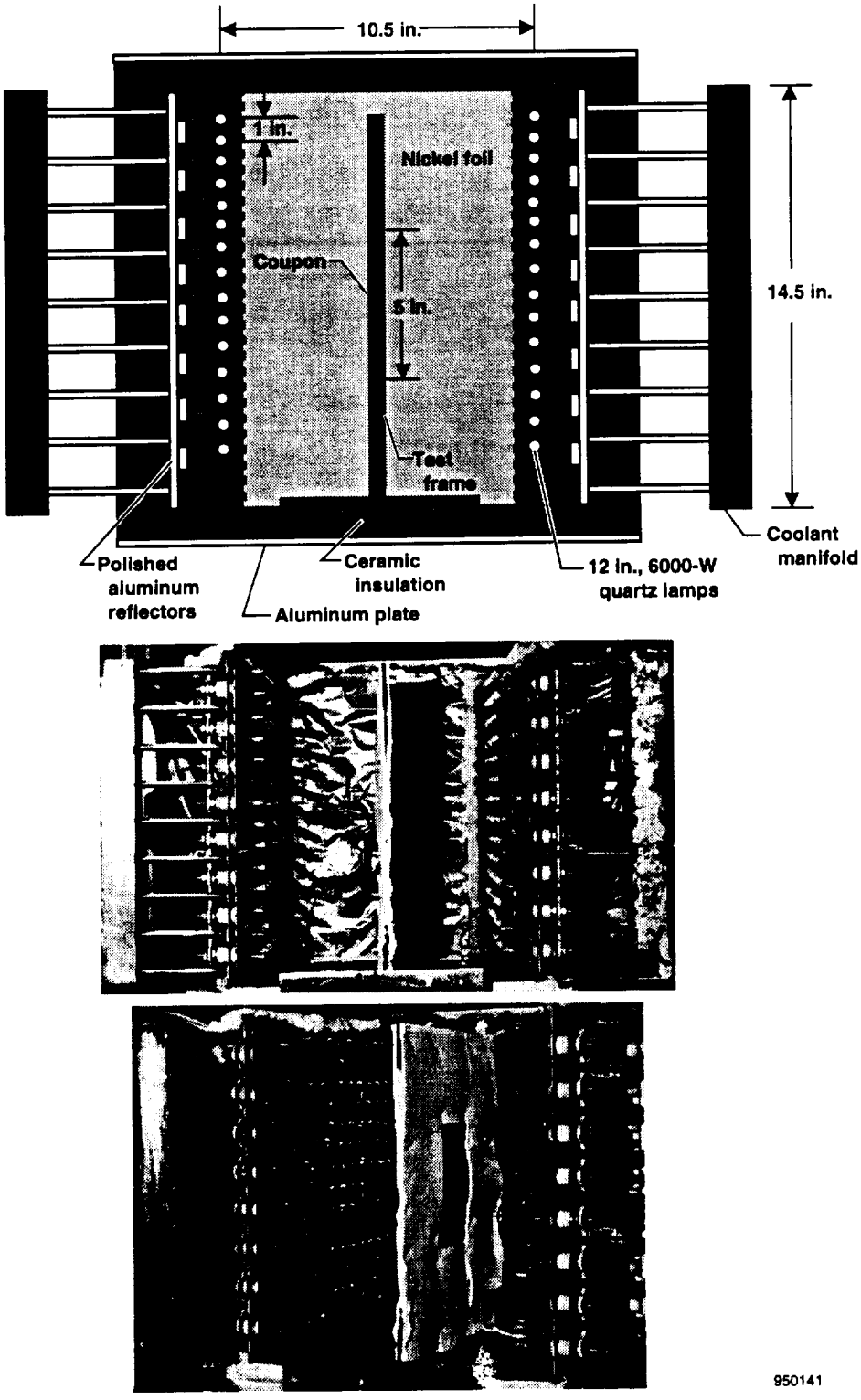

Figure 9. High heating rate oven.

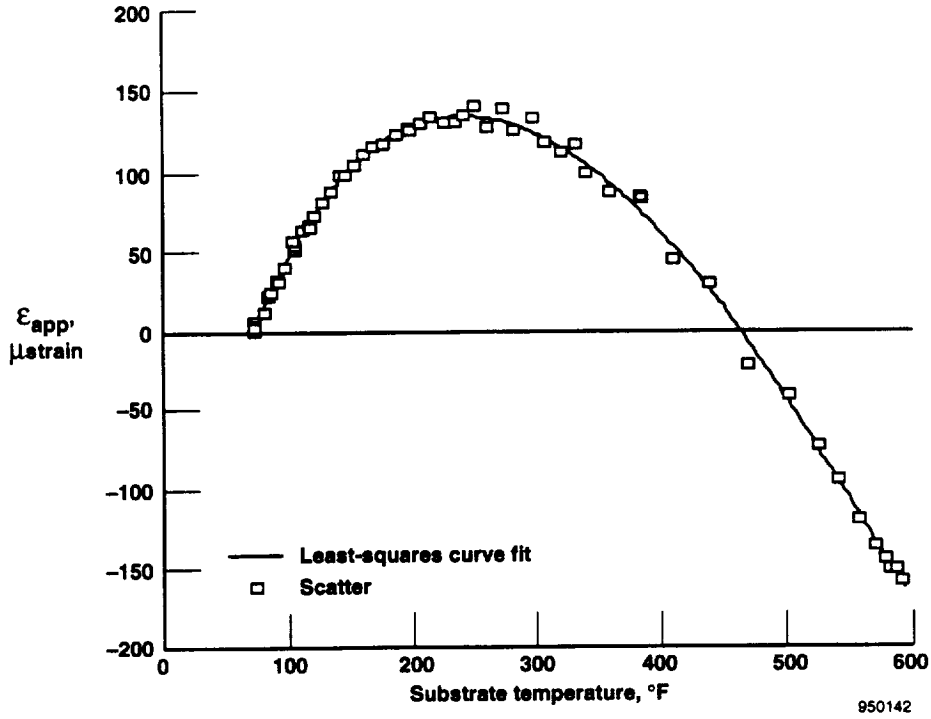

Figure 10. Apparent strain of single strain gage over multiple thermal cycles at 0.3 °F/sec.

Next, the instrumented coupon was subjected to a nominal 80 °F/sec transient-heating profile. Measurements were acquired of ΔT_g, ΔT_s, and ε_{ind} during the profile. This test experienced poor thermal control during the temperature ramp and controlled the coupon surface temperature to ±25 °F of the programmed temperature.

Figure 11 shows the measured temperature profile and a representative strain-gage response as functions of time. This figure demonstrates the sensitivity of the ε_{ind} output to the specific heating profile applied to the coupon. For example, a small rate-of-change in temperature occurs at 2 sec that produces a significant change in the ε_{ind} response. This behavior also occurs because of a decrease in temperature-rise rate at approximately 3.5 sec. The abrupt change in strain rate (fig. 11) was caused by the poor thermal control of the substrate.

Figure 12 shows the gage response as a function of its temperature (fig. 11). This figure shows the strain fluctuation at 300 °F. The three responses expressed in equation (4) are contained in the ε_{ind}: ε_σ, ε_{app}, and ε_T.

If these data were corrected with the conventional method summarized in figure 4, the isothermally determined ε_{app} would be subtracted from the ε_{ind} at each temperature in the profile, according to equation (3). The same assumption made in the ε_{app} tests (namely that the gage and substrate are the same temperature) is also made for the transient-heating data. Any differences in temperature between the gage and substrate are neglected in the conventional procedure.

Figure 13 shows how different the substrate and gage temperatures can be in a transient-heating test. This figure shows the temperature-time histories of the foil and substrate thermocouple measurements from the 80 °F/sec test, with a maximum difference of approximately 20 °F. Another important effect (fig. 13) is how the temperature difference between the gage and substrate changes over the profile. The temperature difference between the gage and substrate, ΔT_{gs}, varies significantly throughout the profile but especially between 3.5 and 4.25 sec and again between 6 and 7 sec. These changes greatly influence the ε_T because the ΔT_{gs} term is a multiplying factor in equation (14).

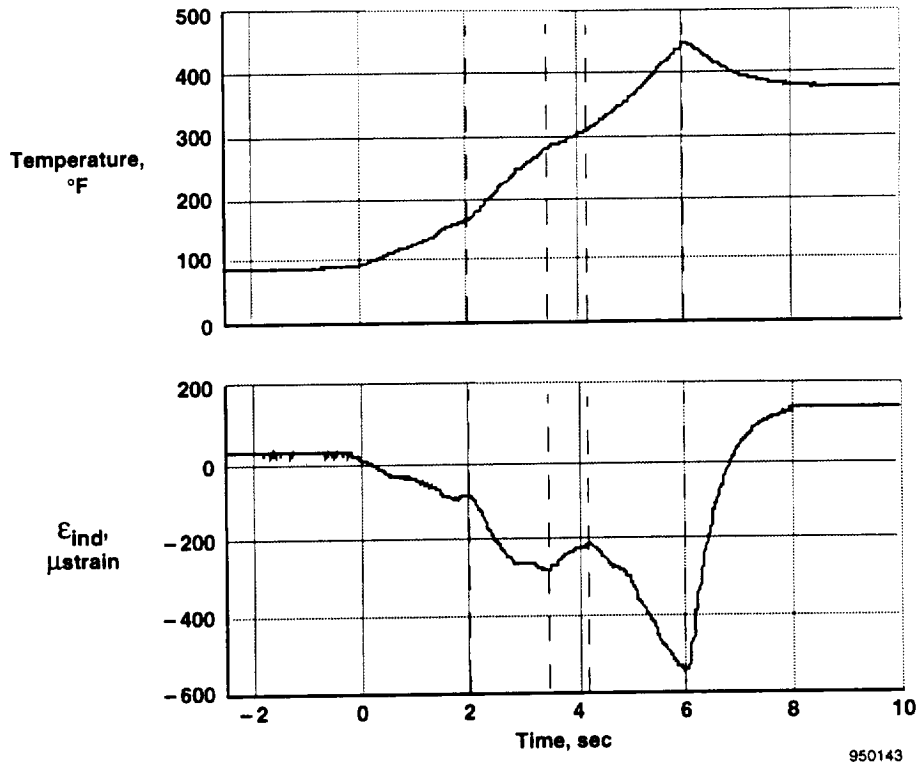

Figure 11. Temperature and indicated strain time histories for 80 °F/sec example.

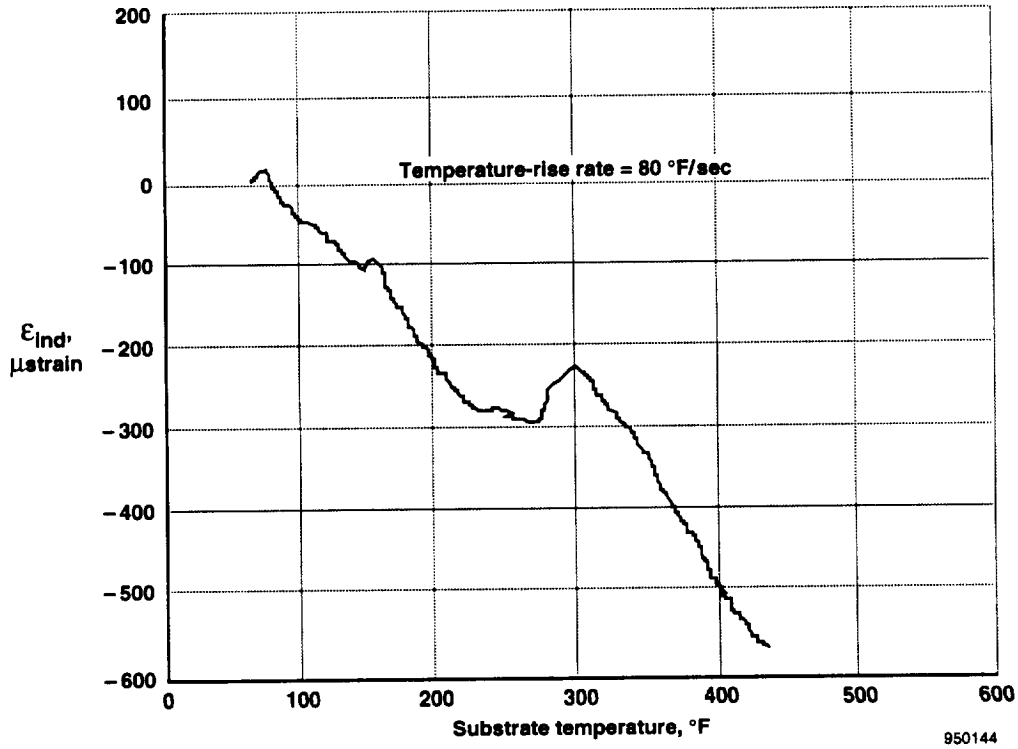

Figure 12. Indicated strain as a function of temperature.

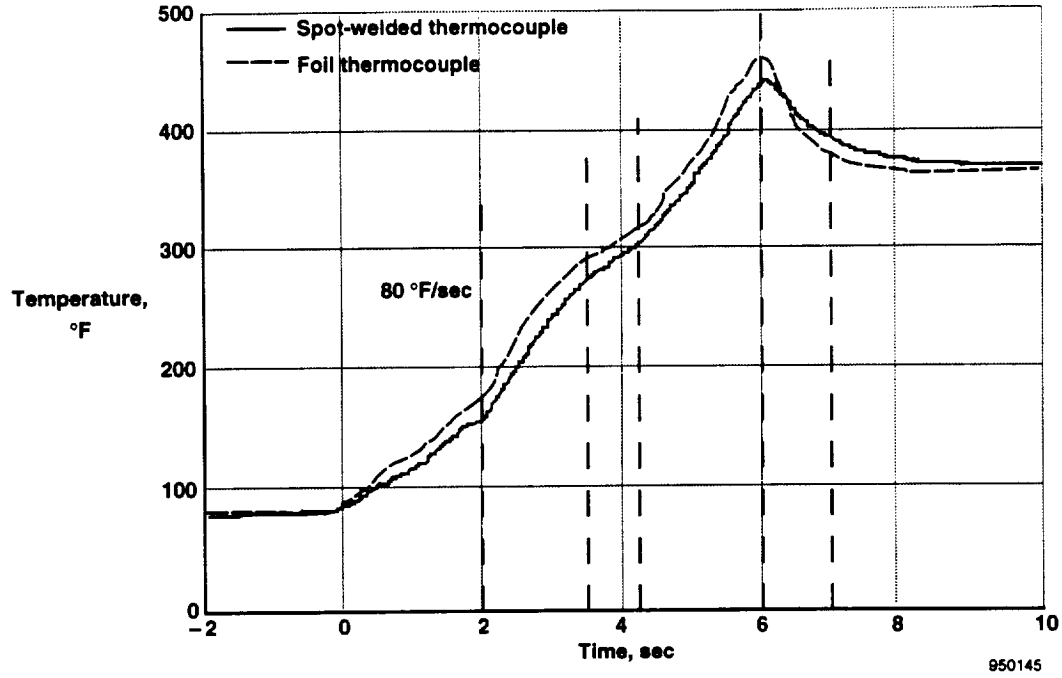

Figure 13. Spot-welded and foil thermocouples as functions of time.

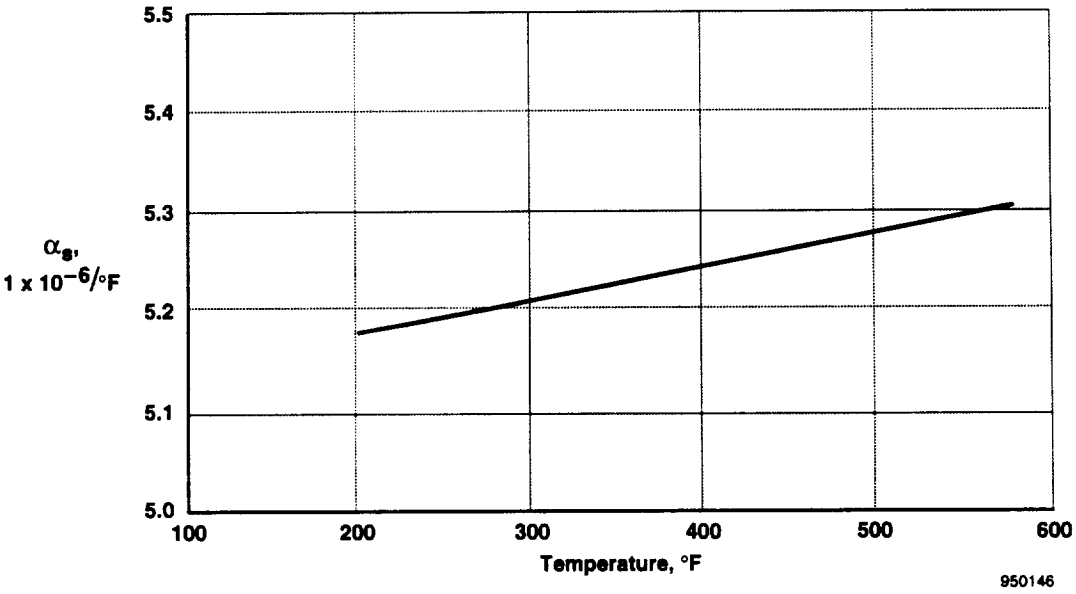

Figure 14. Coefficient of thermal expansion of Ti-5Al-2.5Sn coupon a function of temperature.

The two thermocouple measurements (fig. 13) were input to a FORTRAN computer program. In addition, the ΔT_{gs} term was calculated at each ΔT_s^j in the profile. The ε_{app} (fig. 10) and the temperature-dependent α_s (fig. 14) were also used as input to the program.[10] The first option was then used to compute the ε_T in equation (14). Figure 15 shows the ε_T for this heating test.

The ε_{ind} output for the 80 °F/sec test (fig. 12) is then corrected with both the new and conventional correction procedures to obtain the ε_σ produced in the coupon. Figure 16 shows that, aside from the obvious

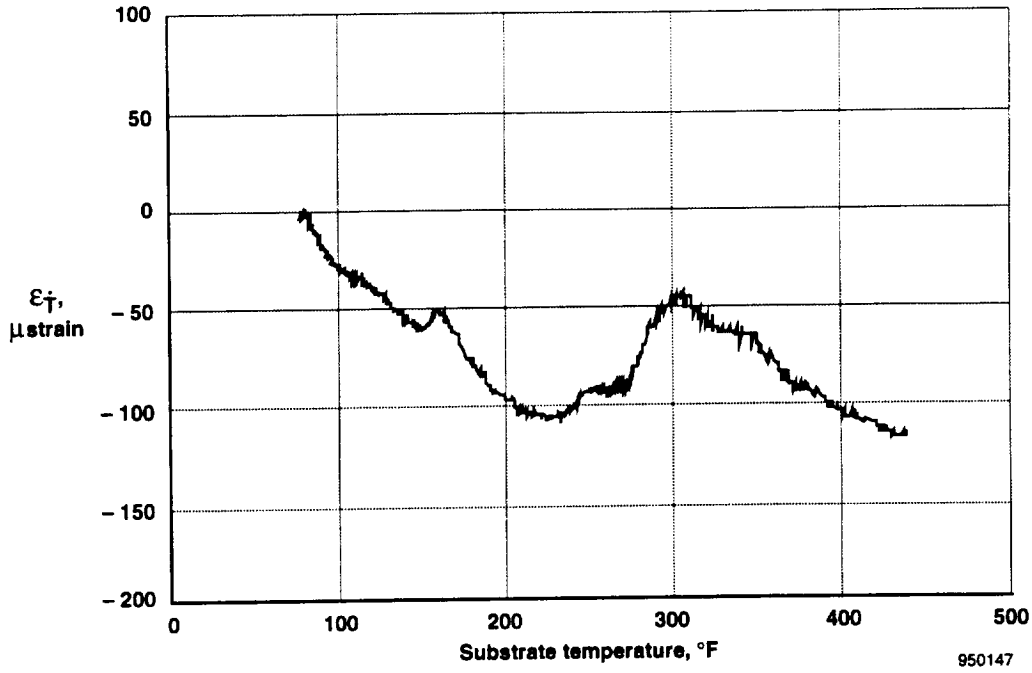

Figure 15. Transient temperature strain error for 80 °F/sec as a function of temperature.

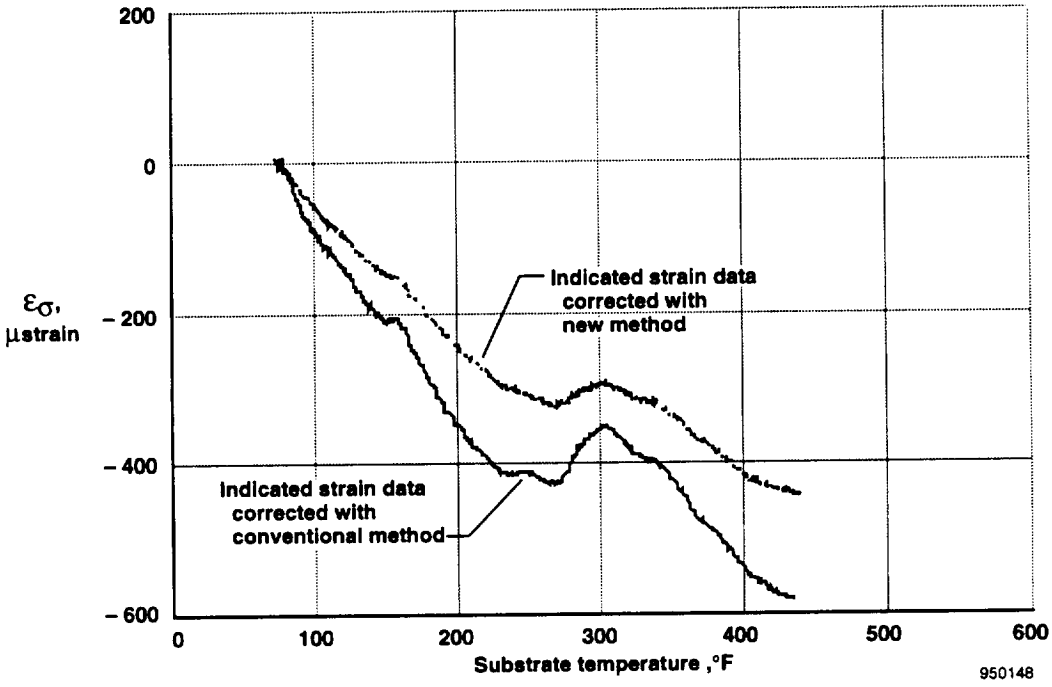

Figure 16. Indicated strain corrected with new and conventional methods.

difference in magnitude between the two curves, the slope changes using the new method are less severe, especially at approximately 300 °F, than the data corrected with the conventional method.

Transient-Temperature Strain Error Results

The first option of the new procedure was also used to determine the transient temperature strain errors for

the other transient-heating tests (fig. 17). These transient temperature strain errors illustrate the significance of the errors that are produced using the conventional correction methods. These errors are especially significant for the 80 and 100 °F/sec tests shown in figure 17(b). For these tests, the magnitude of the $\varepsilon_{\dot{T}}$ is of the same order as the ε_{app} response itself. Because ε_{app} is an error that usually controls the accuracy of strain measurements in elevated temperature conditions, neglecting an error of comparable value may lead to grossly inaccurate strain measurements. Table 2 shows a summary of the transient-temperature strains for a matrix of heating rates and temperatures. Table 3 shows a summary of the ε_{app} error at the same temperatures for comparison.

To provide further insight as to the significance of the transient temperature strain error, the ε_{app} was corrected for gage-factor variation with temperature. The gage-factor error at 600 °F for these gages is less than 3 percent of reading, or approximately 5 μstrain. This error, which is usually corrected, is far less significant than the magnitude of the transient-temperature strain shown in table 2.

Data do not exist at the high-temperature and temperature-rise rates in table 2 because the measured strains at these conditions increased significantly as the heating rate was increased. For example, at 500 °F, some of the ε_{ind} data obtained at high heating rates were approximately −10,000 μstrain and were increasing rapidly. The upper temperature limits proposed for the high temperature-rise rates were, therefore, lowered to avoid exceeding the 15,000 μstrain limit of the gage. Although the upper temperature limit of the strain gage is given by the manufacturer as 550 °F, this limit was not appropriate for temperature-rise rates at or higher than 40 °F/sec. The maximum usage temperatures for these gages were determined to be approximately 500, 450, and 400 °F at temperature-rise rates of 40, 80, and 100 °F/sec, respectively.

Although the correction method presented in this study is intended to be general, the transient-temperature strain results (fig. 17 and table 2) are specific to this study and are presented for qualitative comparisons only. The $\varepsilon_{\dot{T}}$ errors were highly dependent on

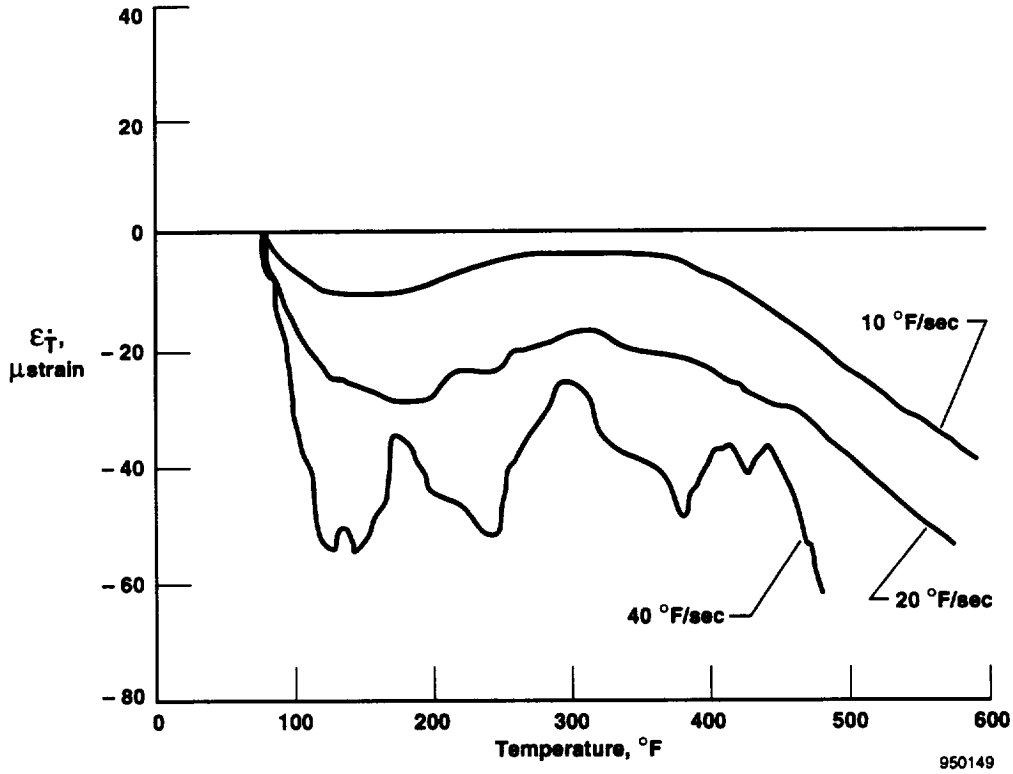

(a) Transient temperature strain error for 10 °F/sec, 20 °F/sec, and 40 °F/sec shown as functions of temperature.

Figure 17. Transient-temperature strain error results.

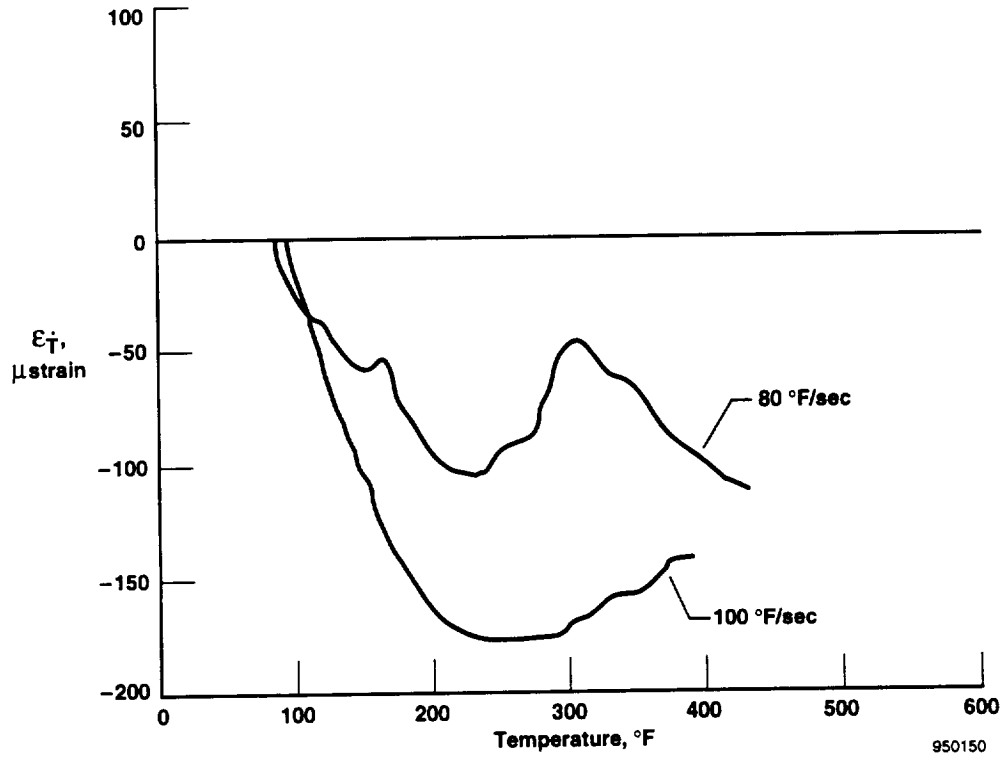

(b) Transient temperature strain error for 80 °F/sec, and 100 °F/sec shown as functions of temperature.

Figure 17. Concluded.

Table 2. Transient-temperature strain errors, $\varepsilon_{\dot{T}}$, for various temperature-rise rates and temperatures.

Nominal temperature-rise rate, °F/sec	Substrate temperatures, °F					
	100	200	300	400	500	600
	Transient-temperature strain error, μstrain					
10	−8	−8	0	−8	−26	−40
20	−16	−28	−18	−26	−40	−56
40	−30	−45	−25	−40	−65	–
80	−30	−95	−50	−100	–	–
100	−15	−165	−170	–	–	–

Table 3. Apparent strain, ε_{app}, for various temperatures.

Nominal temperature-rise rate, °F/sec	Substrate temperatures, °F					
	100	200	300	400	500	600
	Apparent strain, μstrain					
0.3	50	130	125	65	−45	−170

the temperature change of the gage. Because the time constant of the gage is so small, any slight variation in the temperature profile from one test to another will greatly affect the behavior of the error. This fact is clearly illustrated by the fluctuating results in the 40 and 80 °F/sec cases shown in figure 17. For these two cases, the temperature control was especially sporadic, causing the foil thermocouple measurements to lead the spot-welded thermocouple measurements on heating surges and lag during cooling. This wildly fluctuating temperature difference is used to calculate the transient-temperature strain (fig. 17). For these reasons, it is recommended that an indication of the strain-gage temperature be acquired at every strain-gage rosette location during each transient-heating test, especially if the temperature profile varies significantly from one test to another.

ANALYSIS DESCRIPTION

In the previous section, the significance of the errors produced in transient environments for a specific gage installation was established. Test results showed significant differences between new and conventional correction methods. An analysis, however, was required to gain confidence in the experimental results based on the new correction approach.

To accomplish this, the ε_σ in the coupon was determined by first calculating the nonlinear temperature distributions through the coupon using finite-difference analysis. The temperature distributions were then used as input to the closed-form solutions based on thermal stress theory. The analysis described in this section provided calculated surface strains, so comparisons could be made with corrected, measured strains obtained in the experiment.

Finite-Difference Analysis

A one-dimensional, finite-difference model through the thickness of the coupon was created using SINDA '85/FLUINT.[11] Figure 18 shows the model, which was constructed using 11 conduction nodes and 2 boundary nodes. Surface thermocouple measurements throughout each of the transient-heating profiles were prescribed at the two boundary nodes. The interior nodal temperatures were determined at each point in the temperature profile. The temperature dependence of the physical properties of the titanium alloy was considered in the model.

Figure 19 shows an example of the finite-difference results from the same representative 80 °F/sec heating test introduced in the data reduction section. The figure shows a family of temperature distribution curves. Each curve on this plot shows the temperature distribution as a function of the coupon thickness (from –0.125 to 0.125 in.) at a specific time in the profile. The calculated temperatures are shown as symbols at each of the nodal locations.

The same temperature distribution at 6 sec shown in figure 19(a) is also shown in figure 19(b). This figure also shows a third-order curve through the calculated temperatures that was generated using a least-squares regression. As can be seen (fig. 19(b)), the temperature distribution is well-behaved, allowing for a good fit through the data. A similar process was performed on all the other curves (fig. 19) and for all other transient-heating tests.

Theoretical Strain Calculations

The third-order temperature distribution equations resulting from the finite-difference analysis were then used to calculate coupon surface strains at their respective times in the profile. This section develops the necessary equations.

The stress field for a free, unsupported plate with a varying temperature distribution through the thickness is shown. The governing equation is given as[12]

$$\sigma_x = \sigma_y = \frac{1}{1-\nu}\left(-\alpha_s E T(z) + \frac{N_T}{t} + \frac{12M_T}{t^3}z\right) \quad (19a)$$

$$\sigma_{xy} = 0 \quad (19b)$$

where

$$N_T = \alpha_s E \int_{\frac{-t}{2}}^{\frac{t}{2}} T(z)dz \quad (20a)$$

$$M_T = \alpha_s E \int_{\frac{-t}{2}}^{\frac{t}{2}} zT(z)dz \quad (20b)$$

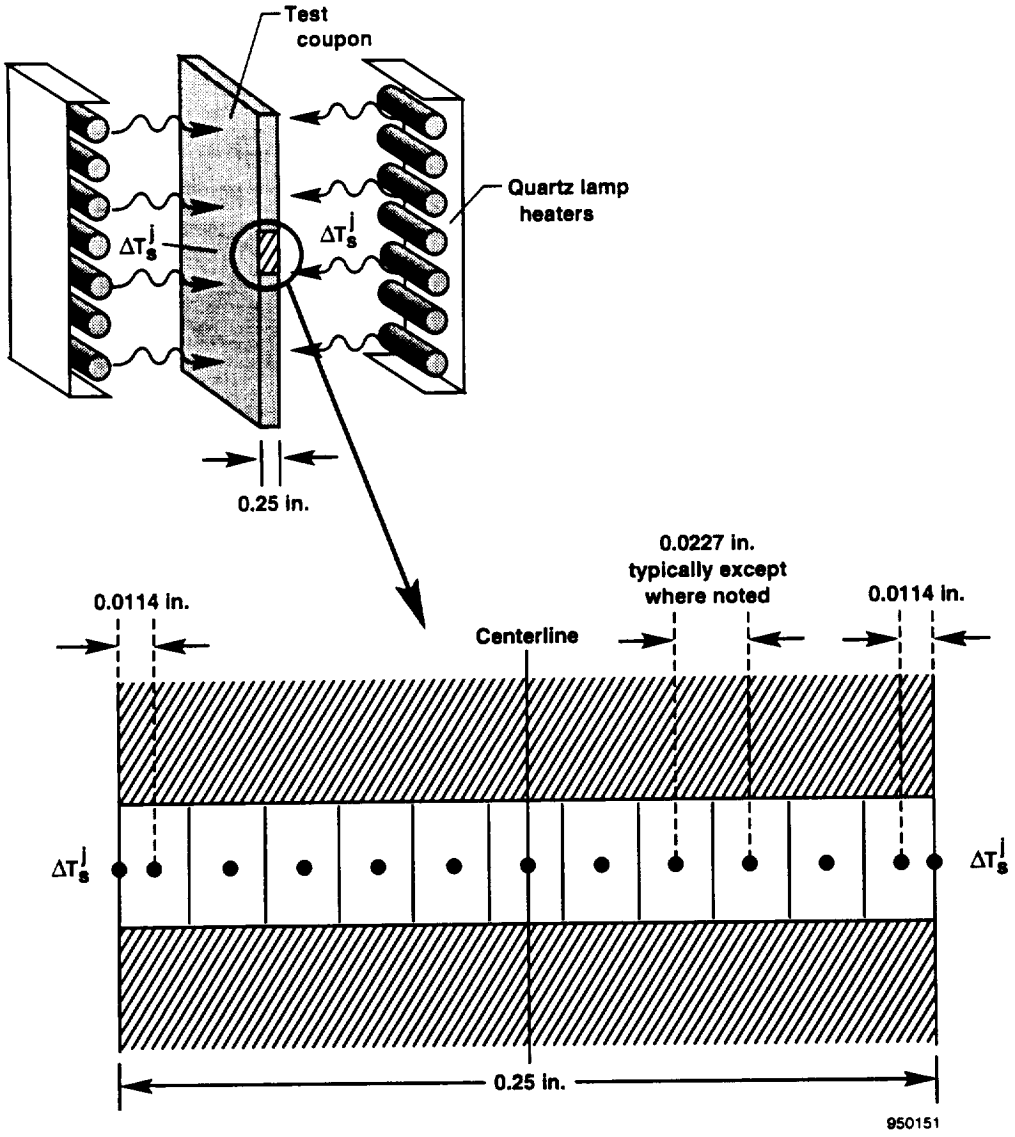

Figure 18. Finite-difference model through the thickness of the coupon.

A general, third-order equation of the form,

$$T(z) = a_0 + a_1 z + a_2 z^2 + a_3 z^3, \tag{21}$$

is substituted into equation (19a) and solved for the following stresses:

$$\sigma_x = \sigma_y = \frac{\alpha_s E}{1-\nu}\left[a_2\left(\frac{1}{12}t^2 - z\right) + a_3\left(\frac{3}{20}t^3 z\right)\right] \tag{22}$$

The stresses in equation (22) are related to strain by generalized Hooke's law. For the specific case where

$$\sigma_x = \sigma_y \text{ and } \sigma_{xy} = 0, \tag{23}$$

Hooke's law becomes

$$\varepsilon_x = \varepsilon_y = \frac{\sigma_x}{E}[1-\nu] \tag{24}$$

The substitution of equation (22) into equation (24) yields principal strains in the plane of the coupon.

$$\varepsilon_x = \varepsilon_y = \alpha_s\left[a_2\left(\frac{1}{12}t^2 - z\right) + a_3\left(\frac{3}{20}t^3 z\right)\right] \tag{25}$$

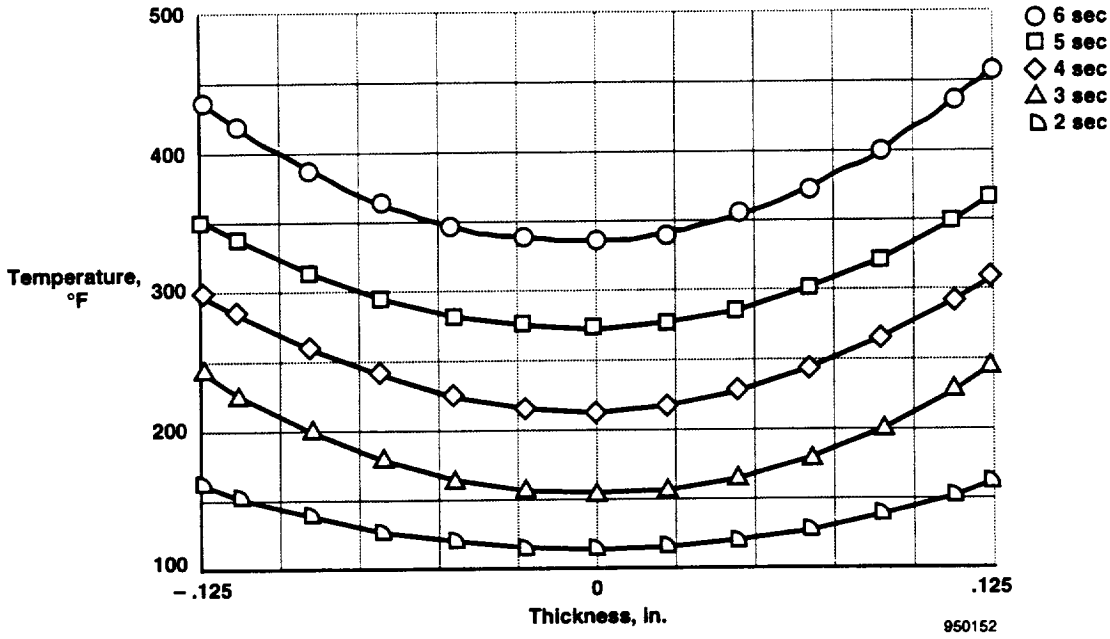

(a) Calculated temperature distributions as functions of thickness and time.

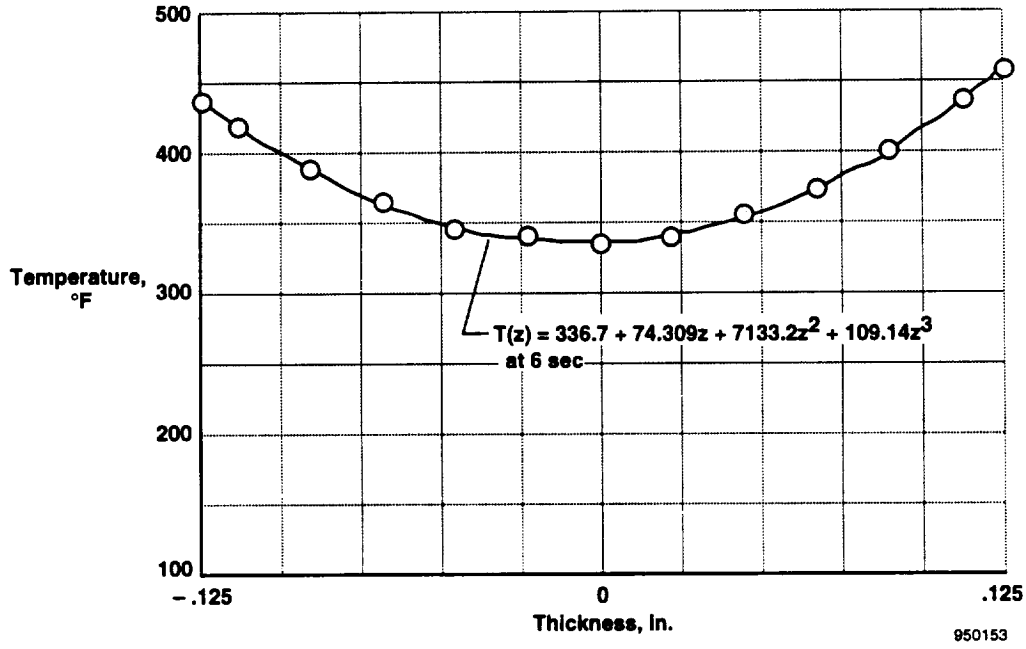

(b) Calculated temperature distributions and a third-order curve fit, at 6 sec as functions of thickness.

Figure 19. Thermal analysis results for 80 °F/sec example.

Equation (25) now provides an expression of the ε_{ind} in terms of a general third-order temperature distribution through the coupon thickness. For this case, the principal strain values calculated from equation (25) can be directly compared with the measured surface strains, ε_{ind}.

The equations of the fitted curves obtained in the finite-difference analysis and the coefficient of thermal expansion of the substrate as a function of temperature (fig. 14) were substituted into equation (25). The surface strains in the coupon were then computed at various times in each of the transient-heating tests.

COMPARISON OF TEST AND ANALYTICAL RESULTS

Figure 20 shows experimental and analytical results for typical tests with temperature-rise rates between 10 and 100 °F/sec. Good correlation between the test and analytical results was obtained for the 20 °F/sec heating rate and greater. The 10 °F/sec case compared moderately well with analysis, given that the temperature difference between the gage and substrate was approximately 2 °F. For the low heating rates, the foil and substrate temperature differences are suspected to be so small that they fall within the uncertainty of the measurement. The results from this case show that no real

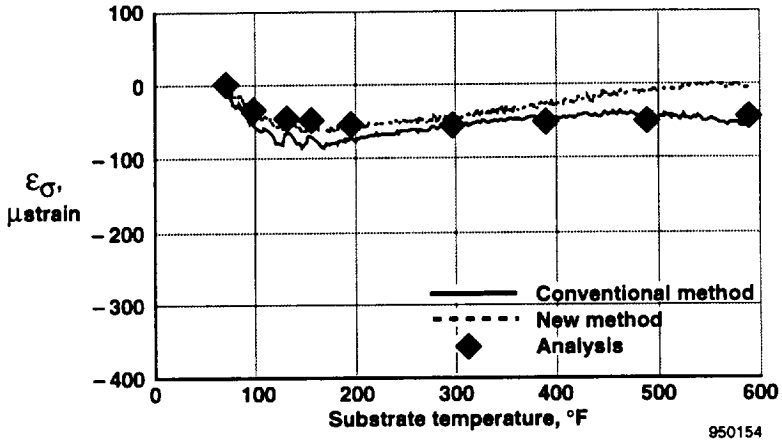

(a) Comparison of stress-induced strain with analysis at 10° F/sec.

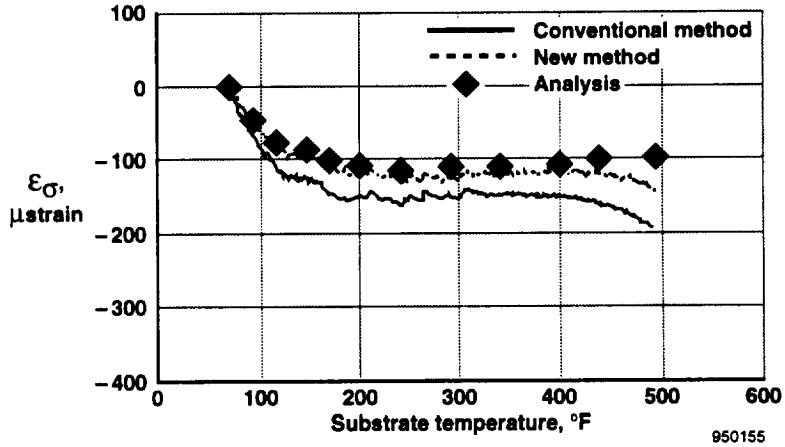

(b) Comparison of stress-induced strain with analysis at 20 °F/sec.

Figure 20. Comparison of stress-induced strain with analysis.

advantage exists in employing the new correction procedure at or below this heating rate.

Figures 20(b) through 20(d) show that applying the new method produced better agreement with analysis than the conventional methods. In the 20, 80, and 100 °F/sec heating tests, excellent agreement between the new method and analysis is shown. Although the new method agreed only moderately well with the 40 °F/sec analysis, the new method was still 27 percent better than results obtained using conventional methods. Strain measurements corrected with the conventional method differed by an average 45 percent from analysis above 300 °F. The 40 °F/sec test result may be caused by a decreased ability to define the ΔT_{gs} term accurately in dynamic heating situations.

During oscillating heating profiles, the foil thermocouple is less capable at effectively representing the foil strain-gage temperature because of the slower response time of the foil thermocouple as compared with the foil strain gage element. The thermocouple foil used in these tests is more than 2.5 times thicker

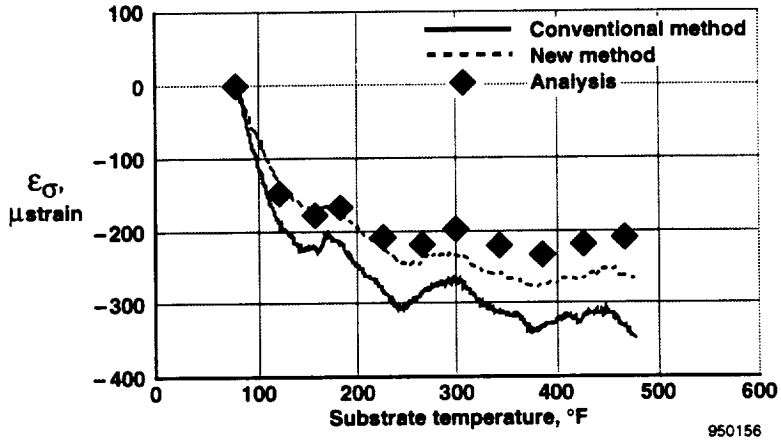

(c) Comparison of stress-induced strain with analysis at 40 °F/sec.

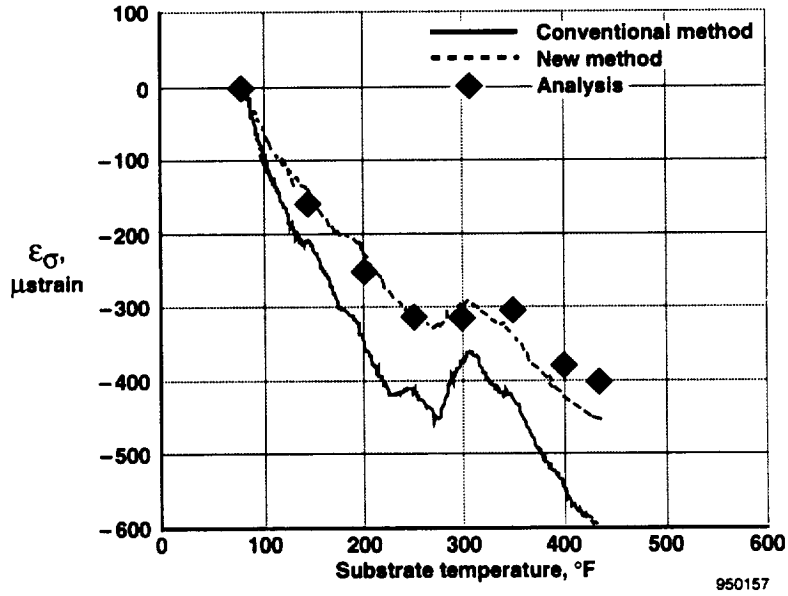

(d) Comparison of stress-induced strain with analysis at 80 °F/sec.

Figure 20. Continued.

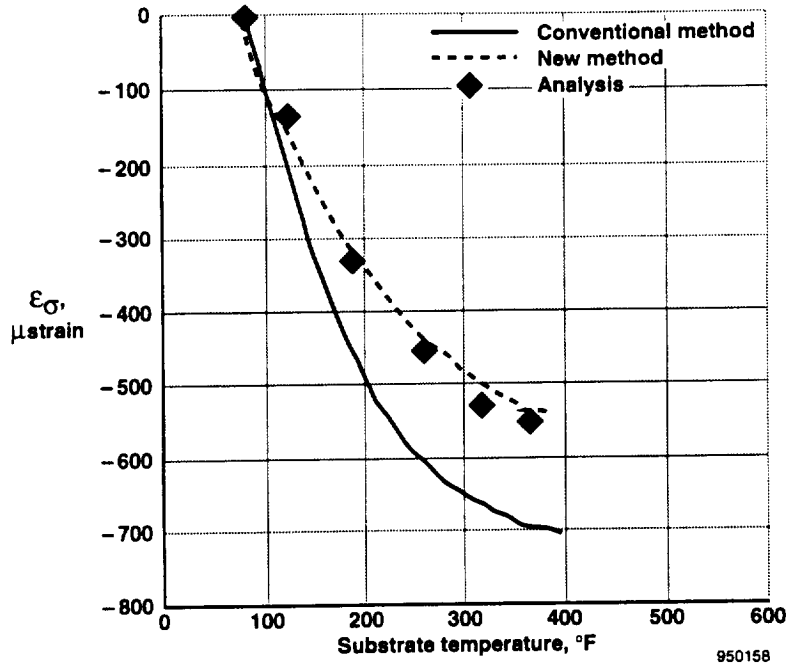

(e) Comparison of stress-induced strain with analysis at 100 °F/sec.

Figure 20. Concluded.

than the strain gage foil (fig. 6). Because the response time (or time constant) is a direct function of the sensor thickness, rapid slope changes in heat flux produce increased temperature lags in the foil thermocouple; therefore, the magnitude of the calculated ΔT_{gs} term is smaller, and in turn, produces smaller ε_T corrections. Even with this temperature lag, however, the new method is still much better than the conventional method for tests with nonideal temperature control or for intentional dynamic heating situations. The results obtained with the new method depend on how well the temperature sensor indicating ΔT_g represents the temperature response of the strain gage.

The test data for the 80 °F/sec heating test, shown in figure 20(d), are the same data presented earlier in the data reduction example (fig.15). Notice that the analytically determined strains in figure 20(d) at 300 °F closely follow measured strains corrected with the new procedure. This agreement shows that the fluctuating strain result at this temperature is the result of real ε_σ in the substrate resulting from the transient-heating profile. The same conclusions hold true for the 40 °F/sec heating test shown, which also had oscillating thermal control.

CONCLUDING REMARKS

A significant strain-measurement error produced in transient-heating environments was mathematically and experimentally defined. The significance of this error was demonstrated for a reliable high-temperature foil strain-gage installation subjected to a variety of radiantly heated, transient-temperature profiles. For temperature-rise rates between 10 and 100 °F/sec, the error resulting from transient heating was as significant as the apparent-strain error. Therefore, for these heating cases, the assumption made in the conventional correction method (that the temperature difference between the strain gage and the substrate is negligible) was not appropriate. For heating rates less than 10 °F/sec, however, the error was negligible. The transient-temperature strain error, which is produced by a temperature difference between the gage and substrate, was extremely sensitive to the specific heating profile applied in a given test.

Although the transient-temperature strain error results were specific to this study, the correction technique used to determine the error is generally applicable to other experimental programs having different heating and instrumentation requirements. The new strain correction technique was developed and successfully demonstrated with analysis. For tests with poor thermal control or dynamic-heating profiles, the new method produced better results than those produced with the conventional method. Conventional methods applied to these conditions deviated from analysis by as much as 45 percent. The accuracy of the new correction method is dictated by how well the strain-gage temperature is represented during the transient-heating profile. For all heating rates greater than 10 °F/sec, the new technique produced strain measurements that compared much better with the analysis than when the conventional technique was used.

REFERENCES

[1]Blosser, Max L., Nowak, Robert J., and Rothgeb, Timothy M., "Thermal-Structural Tests of a Water/Glycol Cooled Aluminum Panel," *Workshop on Correlation of Hot Structures Test Data With Analysis*, NASA CP-3065, vol. I, 1988, pp. 158–178.

[2]Wilson, Earl J., "Installation and Testing of Strain Gages for High-Temperature Aircraft Applications," presented at 1970 Society for Experimental Stress Analysis Fall Meeting, Boston, Massachusetts, Oct. 18–22, 1970, pp. 136+.

[3]Adams, P. H., "Transient Temperature Response of Strain Gages," SAND-80-2689, Rev. 1, Sandia National Laboratory, Albuquerque, New Mexico, July 1983.

[4]Dally, James W. and Riley, William F., *Experimental Stress Analysis, Second Edition*, McGraw-Hill, New York, 1978, pp. 153–178.

[5]Measurements Group, Inc., "Temperature-Induced Apparent Strain and Gage Factor Variation in Strain Gages," Measurements Group TN-504, 1983, pp. 1–7.

[6]Measurements Group, Inc., "Errors Due to Wheatstone Bridge Nonlinearity," Measurements Group TN-507, 1982.

[7]Measurements Group, Inc., "Errors Due to Transverse Sensitivity in Strain Gages," Measurements Group TN-509, 1982.

[8]RdF Corp., "Foil Thermocouples Butt Bonded," Data Sheet No. 36510, *Temperature Measurement Catalog*, Apr. 1991, RdF Corp., Hudson, New Hampshire.

[9]Zamanzadeh, Behzad, Trover, William F., and Anderson, Karl F., "DACS II—A Distributed Thermal/Mechanical Loads Data Acquisition and Control System," presented at the International Telemetering Conference '87, Instrument Society of America, San Diego, California, July 15, 1987.

[10]U.S. Department of Defense, *Military Standardization Handbook: Metallic Materials and Elements for Aerospace Vehicle Structures*, vol. 2, MIL-HDBK-5B, Sept. 1, 1971.

[11]Cullimore, B. A., Goble, R. G., Jensen, C. L., and Ring, S. G., *SINDA '85/FLUINT: Systems Improved Numerical Differencing Analyzer and Fluid Integrator, Version 2.3 User's Manual*, Cosmic Program MSC-21528, Contract NAS9-17448, vol. 1, Martin Marietta Corp., Denver, Colorado, Aug. 1986.

[12]Boley, Bruno A. and Weiner, Jerome H., *Theory of Thermal Stresses*, Robert E. Krieger Publishing, Malabar, Florida, 1985.

Dryden Flight Research Center
National Aeronautics and Space Administration
Edwards, California, February 3, 1995

REPORT DOCUMENTATION PAGE

Form Approved
OMB No. 0704-0188

1. AGENCY USE ONLY (Leave blank)	2. REPORT DATE	3. REPORT TYPE AND DATES COVERED
	March 1996	Technical Paper

4. TITLE AND SUBTITLE

A New Correction Technique for Strain-Gage Measurements Acquired in Transient-Temperature Environments

5. FUNDING NUMBERS

WU 505-70-63

6. AUTHOR(S)

W. Lance Richards

7. PERFORMING ORGANIZATION NAME(S) AND ADDRESS(ES)

NASA Dryden Flight Research Center
P.O. Box 273
Edwards, California 93523-0273

8. PERFORMING ORGANIZATION REPORT NUMBER

H-2043

9. SPONSORING/MONOTORING AGENCY NAME(S) AND ADDRESS(ES)

National Aeronautics and Space Administration
Washington, DC 20546-0001

10. SPONSORING/MONITORING AGENCY REPORT NUMBER

NASA TP-3593

11. SUPPLEMENTARY NOTES

12a. DISTRIBUTION/AVAILABILITY STATEMENT

Unclassified—Unlimited
Subject Category 35

12b. DISTRIBUTION CODE

13. ABSTRACT (Maximum 200 words)

Significant strain-gage errors may exist in measurements acquired in transient-temperature environments if conventional correction methods are applied. As heating or cooling rates increase, temperature gradients between the strain-gage sensor and substrate surface increase proportionally. These temperature gradients introduce strain-measurement errors that are currently neglected in both conventional strain-correction theory and practice. Therefore, the conventional correction theory has been modified to account for these errors. A new experimental method has been developed to correct strain-gage measurements acquired in environments experiencing significant temperature transients. The new correction technique has been demonstrated through a series of tests in which strain measurements were acquired for temperature-rise rates ranging from 1 to greater than 100 °F/sec. Strain-gage data from these tests have been corrected with both the new and conventional methods and then compared with an analysis. Results show that, for temperature-rise rates greater than 10 °F/sec, the strain measurements corrected with the conventional technique produced strain errors that deviated from analysis by as much as 45 percent, whereas results corrected with the new technique were in good agreement with analytical results.

14. SUBJECT TERMS

Apparent strain; Measurement errors; Strain gage instrumentation; Structural testing

15. NUMBER OF PAGES

34

16. PRICE CODE

A03

17. SECURITY CLASSIFICATION OF REPORT	18. SECURITY CLASSIFICATION OF THIS PAGE	19. SECURITY CLASSIFICATION OF ABSTRACT	20. LIMITATION OF ABSTRACT
Unclassified	Unclassified	Unclassified	Unlimited

National Aeronautics and
Space Administration
Code JTT
Washington, D.C. 20546-0001
USA

Official Business
Penalty for Private Use, $300

SPECIAL FOURTH-CLASS RATE
POSTAGE AND FEES PAID
NASA
PERMIT No G27

POSTMASTER: If Undeliverable (Section 158
Postal manual) Do Not Return